Influence of the distribution of expansive sites in aggregates on microscopic damage caused by alkali-silica reaction: Insights into the mechanical origin of expansion

Taito Miura, Stéphane Multon, Yuichiro Kawabata

Title: Influence of the distribution of expansive sites in aggregates on microscopic damage caused by alkali-silica reaction: Insights into the mechanical origin of expansion

Authors: Taito Miura[*1], Stephane Multon[2], Yuichiro Kawabata[3] (* Corresponding Author)

Affiliation:

1: Department of Civil Engineering, Nagoya University, Furo-cho, Chikusa-ku, Nagoya, Aichi, 464-8603, Japan

2: LMDC, Université de Toulouse, INSA/UPS Génie Civil, 135 Avenue de Rangueil, 31077 Toulouse cedex 04, France

3: Port and Airport Research Institute, 3-1-1, Yokosuka, Kanagawa, 239-0826, Japan

Email Addresses: t.miura@civil.nagoya-u.ac.jp (T. Miura), multon@insa-toulouse.fr (S. Multon), kawabata-y@p.mpat.go.jp (Y. Kawabata)

Abstract:

The origin of damage in concrete due to the alkali-silica reaction (ASR) is attributed to the expansion site in the aggregate. To investigate the cracking process of the aggregate during ASR and its consequences on concrete damage, the effect of the distribution of the expansive sites in the aggregate on ASR expansion and the crack patterns must be evaluated. Thus, in this study, a mesoscale discrete model was applied to ASR modeling to represent the propagation of cracking during ASR accurately. The distribution of the expansive sites in the aggregate was based on the gel pocket and reaction rim models, which are two ASR mechanisms reported in the literature. These two expansion models highlight the different crack patterns obtained based on the aggregate characteristics. Further, the expansion

cracking processes determined based on the gel pocket and reaction rim models are consistent with the evolution of cracking with the expansion level.

Keywords: *Alkali-Silica Reaction (ASR), Cracking, Expansion, Expansive site, Mesoscale discrete model*

1. Introduction

When concrete structures are damaged by the alkali-silica reaction (ASR), structural performance is degraded due to the extensive expansion. The ASR expansion is attributed to the dissolution of reactive silica minerals in aggregates that form an alkali-silica gel (ASR gel). A conventional mechanism that induces the expansion of ASR gel is the swelling of ASR gel caused by the imbibition of water [1]. However, the cause behind the expansion of the ASR gel remains controversial [2]. A recent study reported that the water absorption capacity of ASR gels synthesized from concrete is considerably similar to that of calcium silicate hydrate (C-S-H), and the moisture supply to ASR products cannot be held responsible for ASR expansion [3]. Regardless of the ASR gel expansion mechanism, the aggregate and surrounding cement paste demonstrate mechanical responses such as deformation and cracking caused by the expansive pressure exerted by the ASR gel. These responses vary from aggregate to aggregate, and they are dependent on the microstructural localization of the reaction. Thus, it is important to elucidate the effect of the spatial distribution of expansive sites on the microscopic damage in terms of the expansion mechanism.

Several expansion models have been proposed for the microstructural localization of ASR gel expansive sites. Among these models, Ichikawa's model (reaction rim model: the

origin of the expansion is inside the rim in the reactive aggregate [4]) and Dunant's model (gel pocket model: the origin of expansion is randomly distributed inside the aggregate [5]) present two different approaches based on the microscopic observations of aggregates with different petrographic characteristics [4–7]. Both models assume that expansive pressure is exerted at the reaction site (in situ expansion at the reaction site) when the site is well constrained.

The precise modeling of cracking in aggregate and concrete during ASR requires the use of mesoscale discrete models. In this study, a mesoscale discrete model was used to model the aggregate particles and mortar phase. The model was developed based on a 3D-Rigid Body Spring Model (3D-RBSM) [8]. The use of mesoscale modeling for quasi-brittle materials can lead to numerical instabilities. However, 3D-RBSM is a powerful tool for evaluating damage mechanisms related to cracks with high stability and accuracy [8]. Using this model, the effect of the spatial distribution of the expansive sites on microscopic damage—especially cracking propagation due to ASR—was investigated based on the leading ASR expansion models.

2. Literature Review and Analytical Objectives

2.1 Evidence from petrographic observations

2.1.1 Spatial location of expansion

ASR expansion is accompanied by cracking in the aggregate and paste. Cracking patterns differ and depend on the types of reactive aggregates. The current understanding is that confinement is necessary for the ASR gel to exert expansive pressure, and the aggregate itself plays this role; thus, the expansive pressure always increases within the aggregate and the cracks originate from the aggregate and extend to the paste.

After the cracking of the aggregate, the ASR gel may be free from confinement. While the ASR gel can exude through the cracks without expansion, a substitutional reaction between Na and Ca occurs simultaneously [4, 9]. This reaction results in the solidification of the ASR gel in the cracks. Kawabata et al. [9] reported that the solidified ASR gel (similar to C-S-H gel) provides further confinement. The solidification of ASR gel at the interface prevents additional ASR gel from exuding from the aggregate, and this can result in an accumulation of pressure and lead to further crack opening/propagation. A recent study by Shi et al. suggested the possibility that the formation of Ca-rich ASR products at the interface act as a plug that restrains the extrusion of ASR gel [10].

2.1.2 Crack pattern inside the aggregate

Cracks within the aggregate provide important information that can help indicate the location of the origin of the expansion. With respect to the crack pattern inside the aggregate, Sanchez et al. [11] attempted to classify the types of cracks inside aggregates based on the type of reactive rocks. Based on prior research, they divided the cracking mechanism into three types: 1) reaction at the interfacial transition zone (ITZ) of nonporous aggregates; 2) reaction caused by the diffusion of alkali in the aggregate; and 3) reaction at the vein where dissolution of silica occurs inside aggregates [12]. Models studied in the present study were classified according to 2). Further, Sanchez et al. proposed an evaluation of the advancement of the ASR cracking process inside an aggregate using an expansion level. Two types of cracks are observed: a “sharp crack” and an “onion skin crack”. Sharp cracks are likely to pass through aggregates while an onion skin crack propagates in the circumferential direction of aggregates. As the expansion strain increases, sharp cracks propagate into adjacent parts of the aggregate or into the surrounding cement paste, thereby forming a crack network. For onion skin cracks,

the crack reaches the ITZ and propagates into the cement paste. Sanchez et al. commented that these cracks would not always be generated simultaneously. The type of crack—either sharp or onion skin—is dependent on the type of rock. Their observations indicated that sharp cracks can be easily observed in sedimentary and metamorphic rocks. The crack is then easily generated at the porous areas of the aggregate. However, onion skin cracks can be observed when alkali metal ions diffuse uniformly into the aggregate. Based on the experimental results of Ichikawa et al. [4] and Kawabata et al. [9], onion skin cracks tend to appear with highly reactive andesite.

2.2 ASR expansion-mechanism-based models

As indicated in the former section, different distributions of the origin of expansion in aggregates caused by the type of rock strongly influence the ASR mechanisms. In particular, the ASR gel accumulates at certain sites inside the aggregate with increasing pressure, thereby leading to the manifestation of cracks. However, an important question that needs to be emphasized on is the link between the origins of the expansive pressure and the resulting crack pattern inside the aggregate. Thus, the clarification of the manifestation mechanism of aggregate cracking leads to a discussion of the origins of expansion inside the aggregate, and this knowledge can reinforce the understanding of the ASR expansion mechanism.

Two mechanism-based models of ASR expansion can be used to explain how the expansion pressure is exerted within the aggregate: the gel pocket model and the reaction rim model. In the gel pocket model, the random location of a reactive site—a “gel pocket”—is explicitly defined; expansive pressure forms at this gel pocket. In contrast, in the reaction rim model, the heterogeneity of the reactive aggregate is not considered, instead the reaction rim

that forms at the inner surface of the aggregate is considered. Expansive pressure is exerted inside the reaction rim. The details of these models are described with reference to experimental observations below.

The evidence for the gel pocket model has been found from extensive experimental data using SEM images (e.g., Ben Haha et al. [6] and Ponce et al. [7]). These experimental observations indicate that reactive phases presumed as the origins of expansion are randomly distributed inside an aggregate.

In the reaction rim model [4], expansion is the consequence of the diffusion of alkali and ASR-gels of different compositions. First, based on the surface reactions, Na-rich ASR gel is produced by the reaction between alkalis and reactive aggregate. Second, a Ca-rich ASR gel is produced by replacing the Na in the ASR gel with Ca from the paste. The Ca-rich ASR gel is relatively dense and of similar composition to C-S-H, thereby forming a reaction rim at the inner surface of the reactive aggregate. The reaction rim only permits alkali metal ions to transfer into the aggregate; the transfer of the Na-rich ASR gel precipitated inside the aggregate to the outside of the rim is not permitted. Because of further penetration of the alkali metal ions into the inner aggregate, the Na-rich ASR gel accumulates inside the rim and the expansion pressure is exerted gradually. This expansion pressure induces cracks inside the aggregate uniformly, and the crack propagates to the mortar.

2.3 ASR material modeling

Analytical methods for simulating the ASR expansion behavior at the material scale with advanced models have been proposed in the literature [13–21], with the current modeling

138 focused on chemical aspects, mechanical aspects, or a combination of chemical and
139 mechanical mechanisms.

140 ASR advancement can be evaluated in terms of factors of influence related to the ASR
141 gel production process (i.e., amount of alkalis, reactive silica, calcium, temperature, and
142 humidity). Modeling the reaction process often assumes a progression from the aggregate
143 surface to the core, similar to an external attack where transport would be predominant.
144 However, recent developments have demonstrated the importance of considering the
145 combination of alkali and moisture transport with the kinetics of reactive mechanisms [18, 21]
146 to be representative of the observations of damaged concrete [6, 7]. Macroscopic expansion is
147 then calculated according to the change in the amount of ASR gel over time to evaluate the
148 range of expansion strain or induced pressure.

149 At the material scale, differences between the models are caused by the method used
150 to describe the concrete. As concrete is a multiphasic material, macroscopic expansion can be
151 calculated based on different numerical approaches using homogenization principles or a
152 discretization of the material. The accuracy of the estimated expansion and cracking depends
153 on the precision of the concrete description and the combination of known ASR-phenomena.

154 The objective of homogenization approaches is to obtain a numerical assessment of
155 expansion and damage [16, 19] that can be integrated into nonlinear finite element models to
156 assess the structural performance of ASR-damaged structures. With mesoscale discrete
157 models, aggregate particles are directly meshed and modeled to reproduce and comprehend
158 the mechanisms of ASR-induced cracking at the material scale [5, 22–27]. This method is a
159 powerful tool to model macroscopic expansion and analyze the progression of expansion
160 cracks with ASR evolution. Mesoscale discrete models can evaluate the impact of aggregates

(such as distribution, size, and arrangement), the mechanical interaction between aggregate particles, and the distribution of expansive sites in the aggregate on ASR. Mesoscale modeling has been used to reproduce the crack propagation process generated by gel pockets in aggregate particles [5] according to aggregate size [22], stress effect [23], and the impact of creep on ASR expansion [24]. Three-dimensional aggregate particles were modeled with 3D-RBSM to reproduce the crack propagation in the mortar phase between aggregate particles during ASR [26]. In that work, an expansion strain was applied to the boundary between the aggregate and mortar phases. This assumption is representative of certain highly reactive particles. For most moderate or slowly reactive aggregates, cracks were observed inside aggregate particles [6, 7, 11]. The effect of the distribution of reactive sites in the aggregate can impact crack propagation during ASR, and therefore, it must be analyzed via mesoscale modeling.

2.4 Objectives of the analytical approach

As described in the literature review, the crack pattern varies according to the type of reactive rock and expansive site distribution in the aggregate. This difference is attributable to the location of the origins of expansion in aggregates and to the speed of the flow of alkalis in reaching these different locations [21]. The distributions of ASR-crack patterns in concrete and aggregate have significant consequences on the damage induced by ASR at the structural scale.

The first objective of this work is to use a mesoscale model to evaluate the capacity of ASR mechanisms (gel pocket and reaction rim models) to reproduce the crack patterns, as both models are individually described in the literature. The relationship between the

184 macroscopic ASR expansion and internal damage of the aggregate and paste is often
185 questioned in the literature. The nature of the aggregate and the distribution of reactive sites is
186 considered responsible for the difference in damage observed in the literature for equal levels
187 of ASR expansion.

188 The second objective of this work is to compare the crack patterns obtained for different
189 expansion levels by mesoscale modeling with experimental observations from the literature.
190 The crack patterns obtained by mesoscale modeling under different assumptions can help
191 understand this issue.

192 In this study, the influence of the distribution of expansive sites on the cracking process
193 was investigated from a mechanical point of view using a mesoscale discrete model. As the
194 expansion progresses, the influence of the change in the physical properties of the ASR gel in
195 cracks corresponding to the substitutional reaction between Na and Ca becomes more
196 important. The inherent time-dependent behavior such as the creep of cementitious material
197 becomes more pronounced with an increase in induced stress. In the early stage expansion,
198 the ASR gel is well confined by the surrounding minerals or reaction rim. After cracking, the
199 expansion behavior differs from the early stage because the ASR gel tends to flow without
200 exerting expansive pressure when free space is available. At this stage, the stress generated
201 by the rheological behavior of the ASR gel is significantly lower than the mechanical
202 confinement stress, and the change in the physical properties of the ASR gel in cracks has a
203 negligible effect on the initiation of the cracking process. In terms of creep, aggregate cracking
204 is not considerably affected for typical reactive rocks because most of these rocks have
205 negligible time-dependent behavior. In this study, the authors assessed the crack propagation

process in the early stage of expansion caused by the different distribution of the expansive sites in the absence of those influences.

3. Mesoscopic Modeling Approach

In this study, a mesoscale discrete model that expressly represents concrete material by aggregate particles and a mortar phase using a 3D-Rigid Body Spring Model was developed to analyze the ASR cracking process inside aggregates and between adjacent aggregates because of varying distributions of expansive sites in the aggregate. The 3D-RBSM allows mesoscale structural analysis and a powerful tool for comprehending the phenomena related to cracks as it can explicitly evaluate crack width and distribution [28]. The author has previously developed a 3D-RBSM for investigating the mechanism of concrete failure and deterioration involved in cracking such as in the shear failure of RC members [29], rebar corrosion [30, 31], drying shrinkage [32], and external sulfate attack [33]. In this section, an overview of the 3D-RBSM and ASR expansion model using the multi-aggregate model is presented.

3.1 3D-Rigid Body Spring Model (3D-RBSM)

The RBSM is a discrete model proposed by Kawai [28] and it is used for describing cracks. The RBSM is composed of rigid body elements with mechanical springs, which represent nonlinear constitutive laws of cementitious materials placed at the boundary surface between rigid body elements. The rigid body elements are discretized using random Voronoi particles to reduce element size dependency [34] as shown in Figure 1. A mesoscale material constitutive law corresponding to the element size is introduced to mechanical springs so that

macroscopic mechanical behaviors are reproduced where the mechanical springs are comprised of one normal spring and two shear springs arranged at integral points on the boundary surface. Figure 2 shows the tensile, compressive, and shear constitutive laws [8]. The strain of the normal spring is defined as a change in the distance between the center of gravity of adjacent elements with the normal spring behavior corresponding to this strain based on tensile and compressive constitutive laws. For the tensile constitutive law (Figure 2 (a)), the normal spring behaves linearly based on the elastic modulus E until reaching the tensile strength with tensile softening behavior defined by the quarter model. As per the compressive constitutive law shown in Figure 2 (b), the nonlinear behavior is described by a quadratic function so that material failure is attributed to only tensile or shear failure. The shear constitutive law shown in Figure 2 (c) is defined by the shear strain given by the two shear springs. The shear springs behave linearly based on their shear stiffness G until they reach their shear strength after which shear softening behavior is incorporated with the shear softening coefficient K until $0.1\tau_f$. The shear softening coefficient K is obtained by the product of the shear stiffness G and softening coefficient β. In addition, shear strength is applied by a Mohr–Coulomb type criterion to consider the stress dependency of the normal spring. The mesoscale parameters for the mesoscale constitutive law introduced to the normal and shear springs are listed in Table 1. Details on the model are provided in [8].

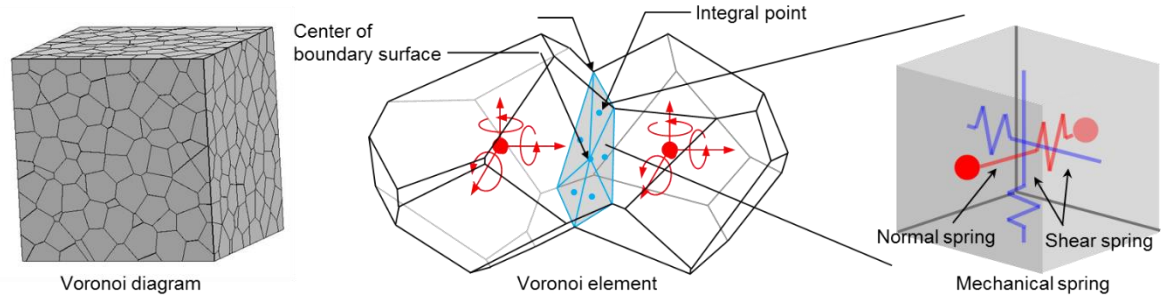

Figure 1 Principle components of the 3D-RBSM: Voronoi elements and the normal and shear springs.

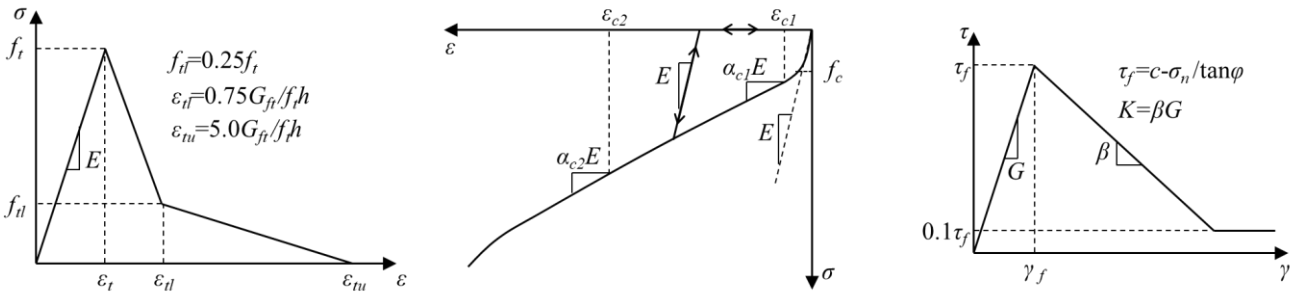

(a) Tensile constitutive law (b) Compressive constitutive law (c) Shear constitutive law

Figure 2 Mesoscale constitutive models for the normal and shear springs.

Table 1 Mesoscale parameters for the mesoscale constitutive law for the normal and shear springs [8].

NORMAL SPRING							
Elastic modulus	Tensile constitutive law		Compressive constitutive law				
E (MPa)	σ_t (MPa)	g_f (N/mm)	f'_c (MPa)	ε_{c1}	ε_{c2}	α_{c1}	α_{c2}
1.4 E^*	0.8 f_t^*	0.5 G_f^*	1.5 f'^*_c	$-2\sigma_c$ $/(E(1+\alpha_{c1}))$	−0.015	0.15	0.25
SHEAR SPRING							
Shear stiffness	Mohr–Coulomb fracture criteria			Softening coefficient			
$\eta = G/E$	c (MPa)	φ	σ_b (MPa)	β_0	β_{max}	X	K
0.35	0.14 f'^*_c	37	f'^*_c	−0.05	−0.02	−0.01	−0.3

* indicates macroscopic mechanical properties.

3.2 Aggregate model

In this study, two models are used for the aggregate as shown in Figure 3: single and the multi-aggregate models.

3.2.1 Single aggregate model

In the single aggregate model, one aggregate is arranged at the center of the analytical model. This model is used to determine the change in cracking behavior inside the aggregate

precisely because of the varying expansive site distributions in the aggregate. The concrete model comprises the aggregate particles and mortar surrounding the aggregates with the analytical model in this case being cubic with a size of 40 × 40 × 40 mm and a 20-mm diameter aggregate placed at the center of the model. The average aggregate element size was 1 mm and the maximum element size for the mortar was 2 mm.

3.2.2 Multi-aggregate model

The multi-aggregate model represents multiple aggregates randomly arranged in the analytical model. This model verifies the crack propagation between adjacent aggregates for varying expansive site distributions. The comparison between single and multi-aggregate models leads to important conclusions on the interest in precisely modeling the distribution of aggregates in concrete to improve the evaluation of ASR expansion and the resulting cracking pattern. The analytical model is a cube with a size of 80 × 80 × 80 mm and 30 aggregates, with diameters of 20 mm, placed randomly in the analytical model. The average element size of the aggregate was 1 mm and the maximum mortar element size was 4 mm. In particular, at least two mortar elements are placed between adjacent aggregates to model crack propagation accurately.

3.2.3 Analysis with proposed models

For two aggregate models, three types of analytical meshes are constructed to assess the variation in expansion behavior because of differences in the arrangement of aggregate and expansive sites. Material parameters for the aggregate phase, mortar phase, and ITZ between these two phases are drawn from the literature and are listed in Table 2.

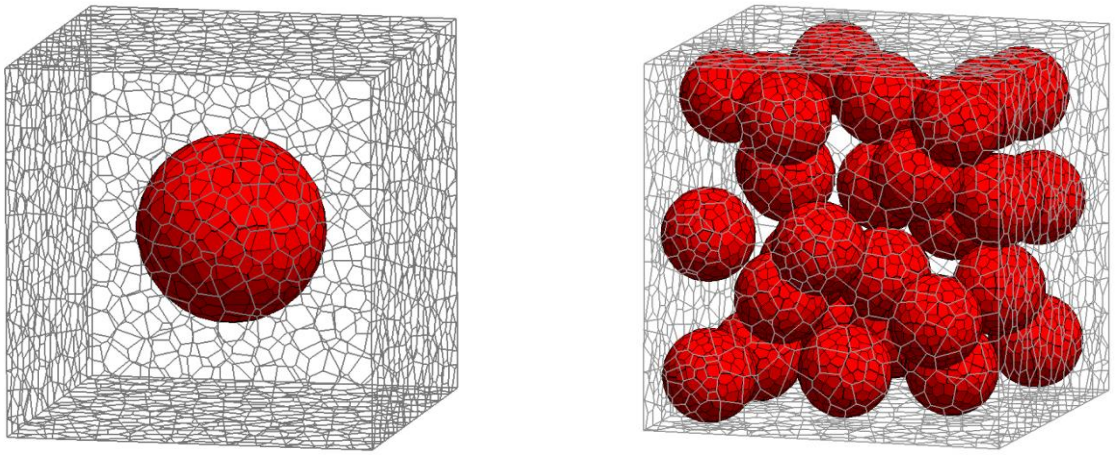

(a) Single aggregate model (b) Multi-aggregate model

Figure 3 Aggregate models in the concrete.

Table 2 Material properties for the mortar and aggregate.

Scale	Material	*fc'* (MPa)	*E* (GPa)	f_t (MPa)	*c* (MPa)	G_f (Nm)
Macro	Aggregate*1	100.0	50.0	11.00	-	-
	Mortar*2	35.0	29.5	2.46	-	0.0559
Meso	Aggregate*3	150.0	70.0	8.80	14.0	0.0005*4
	Mortar*3	52.5	41.3	1.97	4.9	0.0280
	ITZ*5	26.25	20.65	0.98	2.45	0.0140

*1 Material properties for aggregate were based on [5] and [26]. *Fc'* for the aggregate was assumed as 100 MPa.
*2 The compressive strength of the mortar was set to 35 MPa and the other material properties of the mortar were calculated based on the formulation from the JSCE [35].
*3 Mesoscale parameters are applied to calculate the mesoscale constitutive law based on [35] as listed in Table 1.
*4 Fracture energy is unknown. In this analysis, it was applied using a small value as the aggregate cannot represent softening after cracking.
*5 The properties of the ITZ are unknown. This analysis halved the mortar properties, similar to Wang's approach in [26].

3.3 Expansion model

Expansion models used in this analysis are the gel pocket model proposed by Dunant et al. [5] and the reaction rim model proposed by Ichikawa et al. [4]. Physicochemical mechanisms were not considered in this work with the locations of ASR gel expansion (expansive sites) corresponding to the reaction sites even after cracking. Thus, expansive sites are assumed equal to the initial reaction sites.

3.3.1 Gel pocket model

For the gel pocket model, elements containing expansive sites are randomly selected in the aggregate elements assumed to be the microstructural origin of the expansion. Three expansive site ratios in the entire aggregate elements were studied to analyze the effect of the number of aggregate expansive sites on ASR expansion and the cracking mechanisms: 0.5%, 1.0%, and 5.0%. In particular, the aggregate elements containing the expansive sites were randomly selected up to the corresponding volume percentages of all aggregate elements. Thus, the number of expansive sites was decided by the expansive site ratios and the distribution of the expansive sites. The analytical models for the single aggregate model for each expansive site ratio are shown in Figure 4. The expansive site distribution in an aggregate can be randomly arranged (Figure 4, where the visualized expansive site for 5% of the aggregate volume seems to be higher in the plane caused by the visualization problem).

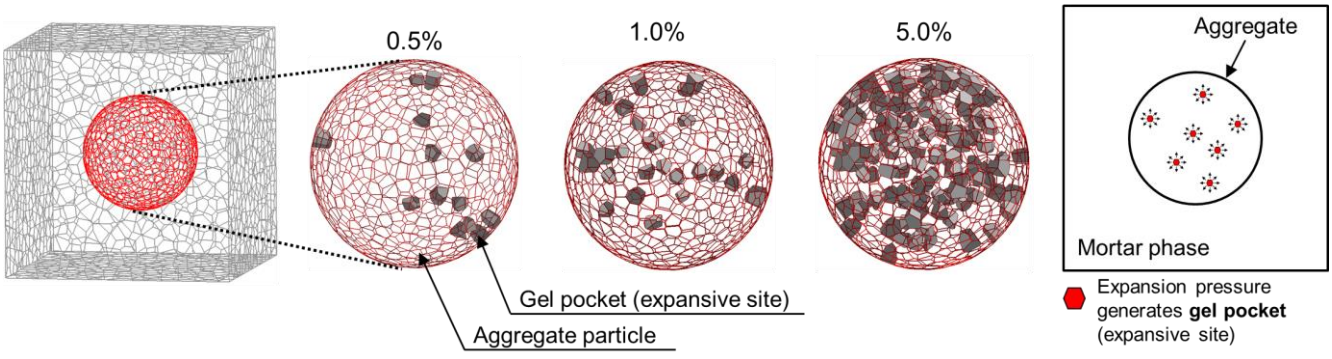

Figure 4 Single aggregate model for the gel pocket model.

3.3.2 Reaction rim model

For the reaction rim model, the expansive sites are considered to form at the inner area of the reaction rim. The location of the expansion pressure inside the aggregate has not been clarified in the literature. Therefore, three types of expansion models were constructed, as shown in Figure 5.

- Boundary model: The thin expansive sites are localized at the inner surface between the reaction rim and the center of the aggregate.
- Layer model: The expansive sites are localized in a thick layer between the reaction rim and the center of the aggregate with a thickness of 2 mm.
- Inner model: The expansive sites uniformly accumulate over the entire inner area of the reaction rim.

The change in the elastic modulus caused by the densification of surface layers owing to rim formation and the change in the thickness of the reaction rim with time were not considered in this model. The thickness of the reaction rim was assumed to be 2 mm based on Ichikawa et al. [4], and it was maintained at 2 mm in all models in this study. Prior to the present study, it was confirmed with a sensitivity analysis that the effect of the thickness of the reaction rim has a slight effect on the crack pattern.

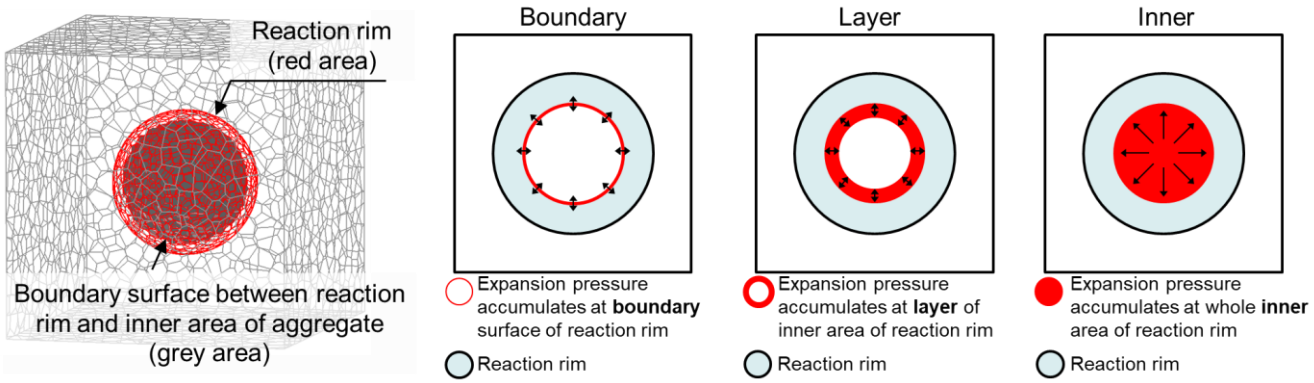

(a) Aggregate model (b) Boundary model (c) Layer model (d) Inner model

Figure 5 Single aggregate model for the reaction rim model: (a) Aggregate model where the surface area is the 2-mm-thick reaction rim and the inner area has an expansibility with different expansive sites; (b) boundary model with thin expansive sites localized at the inner surface between the reaction rim and aggregate center; (c) layer model with expansive sites localized in a thick layer between the reaction rim and aggregate center with a thickness of 2 mm; and (d) inner model where expansion sites uniformly accumulate at the entire inner area of the reaction rim.

3.3.3 Numerical description of the expansive site for the multi-aggregate model

Figure 6 shows the analytical model of the multi-aggregate model for the gel pocket model and reaction rim model with the numerical description used to describe the expansive sites listed in Table 3. The arrangement of the aggregates used for the gel pocket model and the boundary model of the reaction rim model were the same, whereas the arrangement for the layer and inner models varied from those of the other models. This is because the layer and inner models required a spherical volumetric element arrangement in the aggregate. However, it was confirmed that the influence of different aggregate locations in the analytical model on the expansion behavior is negligible for the multi-aggregate model.

Regarding the gel pocket model, the expansive site ratio of the aggregate is the same as that of the single aggregate model. Then, to assess the expansive site distribution of the gel pocket model quantitatively, the average volume corresponding to the expansive site and the average spacing between adjacent expansive sites were calculated as listed in Table 3. The average volume corresponding to the expansive site was derived from the aggregate volume divided by the expansive site element number. For spheres centered on one element of the expansive site with diameters equal to the distance to the closest “expansive site”, the mean sphere diameter was calculated as the average diameter for all expansive sites, thereby giving the average spacing between adjacent expansive sites. According to the expansive site distribution, the average spacing between adjacent expansive sites for expansive site ratios of

0.5, 1.0, and 5.0% are 6.44 mm, 5.22 mm, and 3.12 mm, respectively. Table 3 summarizes the details on how the expansive sites are densely distributed in the aggregate. However, these values are only averages, and they are one of the indices to represent the expansive site distribution.

For the reaction rim model, the expansive site volume ratios of the aggregate for the layer and inner models are 42.17% and 43.56 %, respectively, while the boundary model has no expansive site volume as the expansive site is applied to the boundary surface. These high values of expansive sites are imposed by the geometry of the rim (radius and thickness). In comparison to the gel pocket model, the ratios of the expansive site for the aggregate for the layer and inner models are considerably higher than that of the gel pocket model (between 0.5% and 5.0%). The consequences of the difference in terms of macroscopic expansion and cracking are discussed in Section 4.2.2.

For both expansion models, an expansion strain of 100 μm/m was constantly applied to the normal spring of the expansive site as imposed strains (so-called initial strain in the field of computational dynamics), and it was applied to the single aggregate model. This analytical method for applying the expansion strain is similar to that reported by Wang et al. [26]. As the expansion rate is equal, earlier expansion results for models with the greatest expansive site volume. The viscoelastic behavior of ASR gel will be modeled in future research.

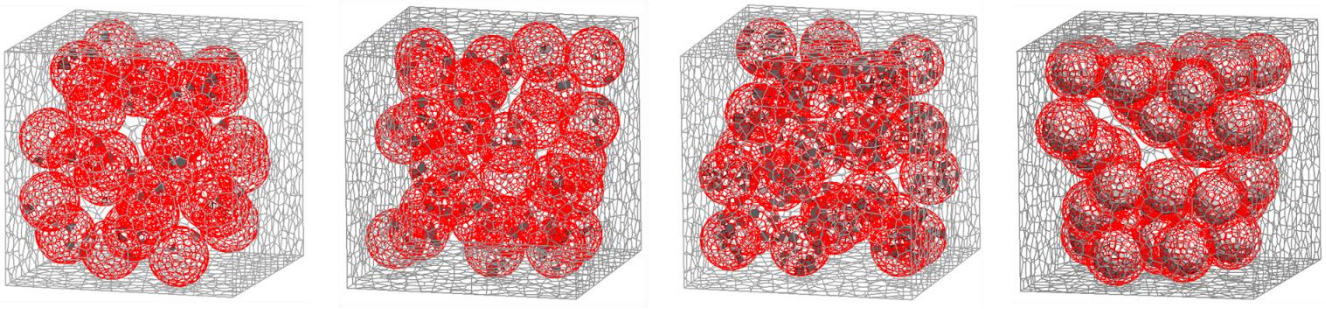

(a) 0.5% (b) 1.0% (d) 5.0% (d) Reaction rim model

Figure 6 Multi-aggregate model for the gel pocket model and reaction rim model; (a), (b), and (c) are the gel pocket model for each expansive site ratio, and (d) is the reaction rim model (three assumptions for the expansive site inside the aggregate as described in Figure 5 are analyzed for the multi-aggregate model).

Table 3 Expansive site details for the multi-aggregate model.

Expansion model	Gel pocket model			Reaction rim model		
	0.5%	1.0%	5.0%	Boundary	Layer	Inner
Total element number	18,064				18,075	18,130
Total volume (mm^3)	512,000					
Aggregate element number	9,559				9,530	9,598
Aggregate Volume (mm^3)	127,768				127,761	127,758
Expansive site element number	52	98	457	-	3,030	3,486
Expansive site volume (mm^3)	709	1,320	5,995	-	53,872	55,653
Vol.% in aggregate	0.56	1.03	4.69	-	42.17	43.56
Average volume of expansive site *1 (mm^3)	2,457.1	1,303.8	279.6	-	-	-
Average spacing of adjacent expansive site *2 (mm)	6.44	5.22	3.12	-	-	-

*1: Average volume of the origin of expansion = aggregate volume / expansive site element number.
*2: Average spacing of adjacent expansive sites is the sphere diameter calculated by average volume of the expansive site.

3.4 Definition of macroscopic expansion strain

In this analysis, the macroscopic expansions in the *x*-, *y*-, and *z*-directions were defined as shown in Figure 7. The macroscopic expansion is the concrete strain, which is the consequence of the cumulative strain applied to the reactive sites. Macroscopic expansion is determined by the model. Four gauge points were placed at four surfaces in the *x*- and *z*-directions, and each gauge point was placed at the element where these elements were 10 mm from the nearest vertex of the surface; the gauge lengths were approximately 20 mm. Two lateral macroscopic expansions in the *y*-direction and two transversal macroscopic expansions in the *x*- and z-directions were defined from the four gauge points of each surface. Therefore, there are eight lateral macroscopic expansions and four transversal macroscopic expansions

in the *x*- and *z*-directions. Thus, the average strain in each direction, lateral macroscopic expansion in the *y*-direction, and transversal macroscopic expansion in the *x*- and *z-directions* can be obtained. The volumetric strain was defined as the summation of the lateral and two transversal macroscopic expansions.

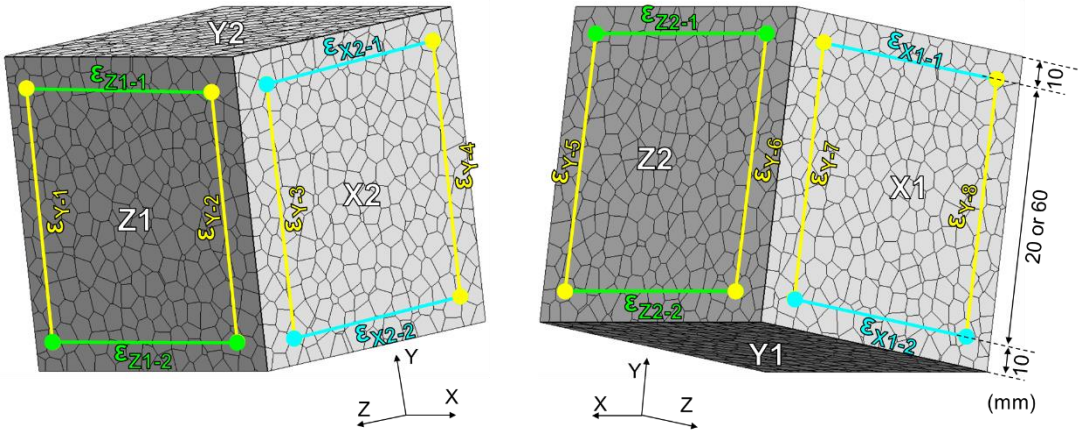

Figure 7 Definition of macroscopic expansion.

4. Numerical Simulations and Results

4.1 Analytical results for the single aggregate model

The change in expansion behavior caused by the different distributions of the expansive site based on the gel pocket and reaction rim models was first verified with the single aggregate model. The process of expansion crack propagation is discussed according to the expansion evolution, deformation, crack distribution, horizontal tensile and vertical compressive stress distributions at the center of the cross-sectional area, which are shown in Figures 8–13. In these figures, the expansion process is indicated by the cumulative applied strain of the expansive sites. The cumulative applied strain is calculated by accumulating the applied strain at one expansive site for each step. For instance, after one-hundred calculation steps, the

418 resulting cumulative applied strain is 1.0 % when the applied strain is 100 μm/m (0.01%) for
419 every step.
420
421 **4.1.1 Gel pocket model**
422 The expansion evolution until the volumetric strain is reached is approximately 0.5% as
423 shown in Figure 8. The cumulative applied strain in the expansive site necessary to reach 0.5%
424 of volumetric expansion in the concrete decreases as the ratio of the expansive site increases
425 (i.e., the cumulative applied strain has to be lower as the expansive site is greater). The
426 expansion in the three coordinate directions demonstrates high anisotropy according to the
427 expansive site distribution; this expansion occurs in one direction and the expansion in the two
428 other directions is close to zero. Thus, the crack propagated in only one direction (Figure 9).
429 This leads to high scattering in the results for directional expansions according to expansive
430 site distribution, while the volumetric strain has only small differences. Therefore, the
431 macroscopic expansion change is considerably constant and the only weakly dependent on
432 the direction of the expansion crack propagation. The macroscopic expansion in the three
433 directions varied widely as a result of the variation in crack propagation direction because of
434 the analytical mesh and arrangement of the expansive sites. In the case of the single aggregate
435 model used for the gel pocket model, once one crack is initiated in one direction, the increase
436 in cumulative applied strain leads to this crack opening without the initiation of new cracks in
437 the other directions.
438 This has already been observed for macro-modeling when perfect plasticity is used to
439 represent ASR expansion. In the case of macro-modeling, this phenomenon has been solved
440 by the addition of a hardening behavior to plasticity induced by ASR expansion [36]. With a

hardening law, the ASR expansion is isotropic under stress-free conditions [37].

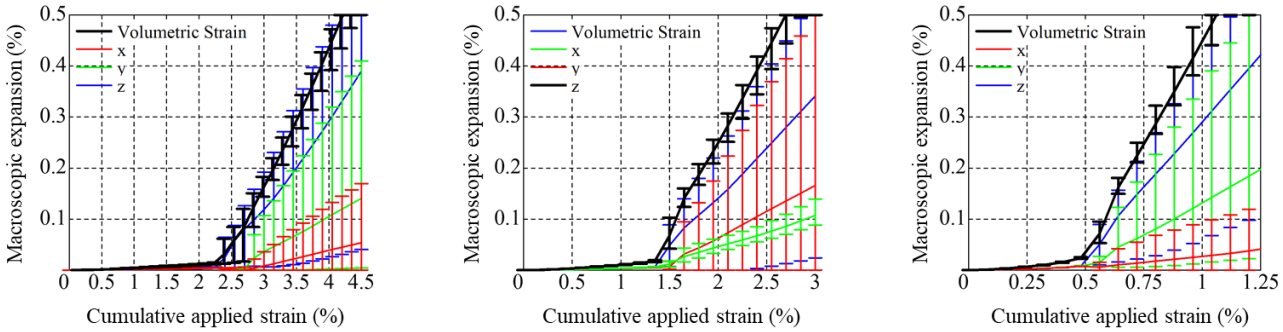

(a) 0.5% (b) 1.0% (c) 5.0%

Figure 8 Concrete expansion evolution with cumulative applied strain of the expansive sites for the gel pocket model for the single aggregate model until a volumetric strain of approximately 0.5% is reached. The error bars are calculated from the three different analytical meshes.

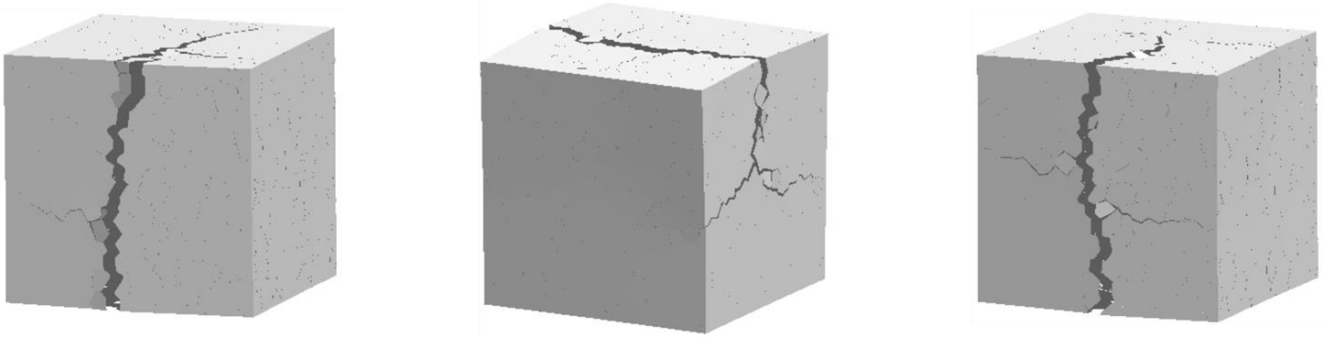

(a) 0.5% (b) 1.0% (c) 5.0%

Figure 9 Deformation of the gel pocket model for the single aggregate model when the volumetric strain reaches approximately 0.5% (magnification is ten times).

Figure 10 presents the crack distribution and horizontal tensile and vertical compressive stresses at the center of the cross-sectional area. Four stages were extracted for the analysis: before cracking, at the generation of crack, after crack propagation, and at approximately 0.5% of the volumetric strain. According to the crack distribution, when the expansive site ratio is lower than 1%, first, cracks are generated inside the aggregate, and subsequently, the cracks

propagate from the mortar to the aggregate. In the case of an expansive site ratio of 5%, the cracks inside the aggregate are finer and fewer, and crack propagation from the mortar to the aggregate occurs at almost the same time. Compressive stresses are generated locally in the expansive sites and they reduce slightly with crack propagation. Before cracking, the unstable stress balance causes localized tensile stress and leads to crack initiation. After cracking, crack propagation is influenced by tensile stress as the orientation of cracking is already determined at the time of initiation. In addition, after cracking, the stresses gradually release, thereby corresponding to crack development. Thus, the compressive stress cannot accumulate up to a higher stress level and affect crack propagation. Tensile stresses are generated close to the expansive site before cracking, and they gradually release as the cracks propagate inside the aggregate and from the mortar to the aggregate. In the case of an expansive site ratio of 5.0%, there are many expansive sites in the aggregate. Compressive stresses in the aggregate appear and increase because of confinement by the cement paste unless local compression failure occurs. During this stress state in the aggregate, the tensile stresses transfer from the aggregate to the mortar, and the tensile stresses at the outer surface reach the tensile strength. Thus, aggregate cracking and cracks propagating from the mortar to the aggregate occur almost simultaneously.

The mechanism behind the unexpected cracking process from the mortar to the aggregate is discussed as follows. First, compressive stresses generated at the expansive sites as the surrounding “nonreactive” aggregate phases inhibit the deformation because of expansion. Simultaneously, tensile stresses are generated at the surrounding aggregate phases corresponding to the generation of compressive stresses, and the internal stresses then become balanced. Further, as the compressive stresses in the expansive sites develop,

482 the surrounding tensile stresses develop and gradually transfer to the external surface.
483 Because of the effect of three-dimensional internal constraints at the inner area, the tensile
484 stresses are difficult to develop though small amounts of damage could be generated. The
485 tensile stresses outside the mortar phase can increase up to the tensile strength as the effect
486 of the internal constraint is smaller or almost zero at the outer surface of the mortar phase as
487 compared to the inner surface. This is why cracks propagating from the mortar to the aggregate
488 can appear, and it should be noted that this crack observed in the single aggregate model is
489 an evident result from the analytical approach. Considering the actual heterogeneity of the
490 aggregate and its shape, stress concentrations could be generated inside the real aggregate.
491 These stress concentrations could manifest as cracks because they promoted the localization
492 of the aggregate cracking and inhibited the uniform tensile stress transfer. Thus, the crack
493 propagating from the mortar to the aggregate—as obtained by the numerical approach—can
494 be explained by the internal constraint effect.

495 Numerical results using the gel pocket model confirmed that the crack pattern has sharp
496 cracks [11] and crack distributions when the expansive site ratio is lower than 1.0% are similar
497 to those of Dunant [5].

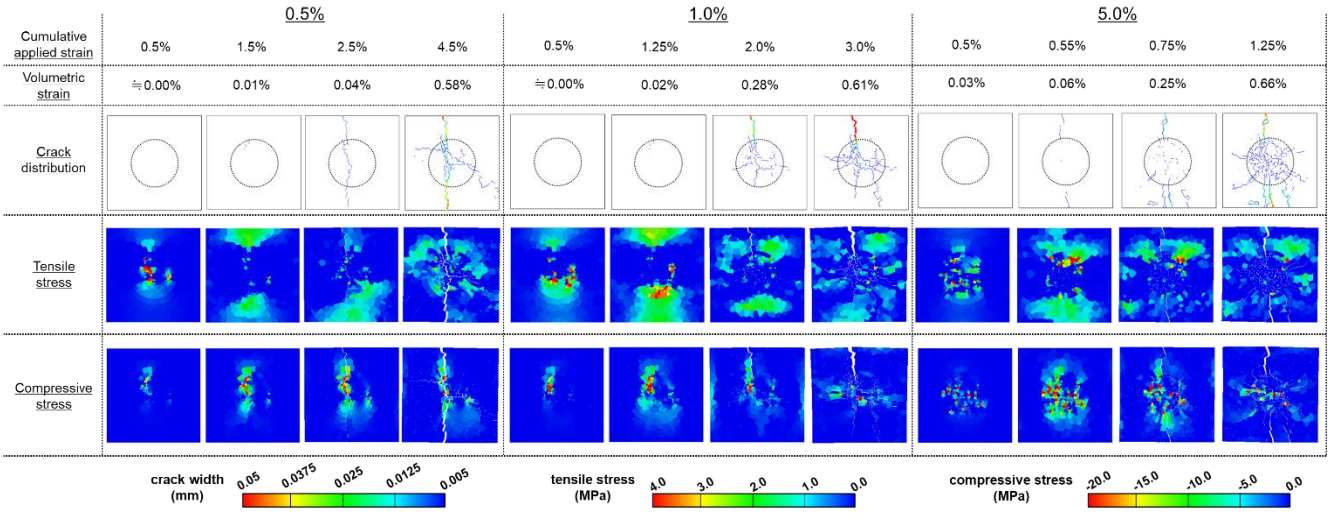

498

Figure 10 Crack distribution and horizontal tensile and vertical compressive stresses at the center of the cross-sectional area of the gel pocket model for the single aggregate model (magnification of the deformation is ten times). The black broken line indicates the boundary surface of the aggregate. The four cumulative applied strain stages represent results before cracking, at the generation of cracking, after crack propagation, and after the volumetric strain reaches 0.5%.

4.1.2 Reaction rim model

The analytical results for the reaction rim model are shown in Figures 11–13. The expansion evolution until the volumetric strain is approximately 0.5% is shown in Figure 11. First, the effect of the assumption of the location of the pressure (boundary, layer, and inner model) is discussed. The boundary model requires a higher cumulative applied strain to reach 0.5% of the volumetric strain, while the cumulative applied strains of the layer and inner models are equal. The variation of the expansion in the three directions and volumetric strain for all cases are similar to the gel pocket model. This is because the expansion cracks propagate in one direction for the single aggregate model as shown in Figure 12.

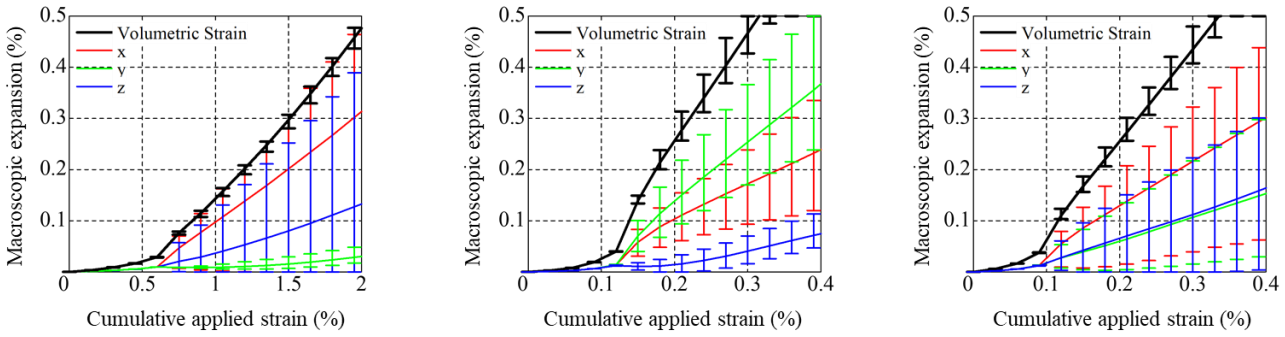

(a) Boundary model (b) Layer model (c) Inner model

Figure 11 Concrete expansion evolution versus cumulative applied strain of expansive sites for the reaction rim model for the single aggregate model up to a volumetric strain of approximately 0.5%. The error bars are calculated from three different analytical meshes.

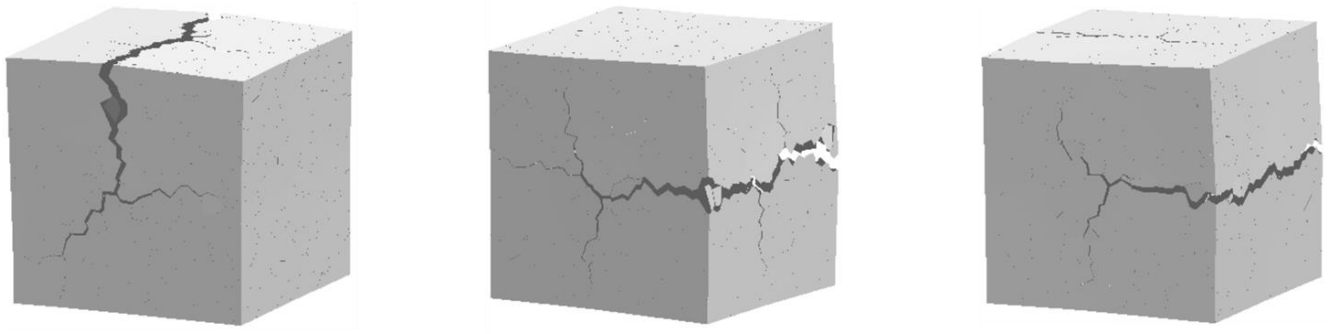

(a) Boundary model (b) Layer model (c) Inner model

Figure 12 Deformation for the reaction rim model for the single aggregate model when the volumetric strain reaches approximately 0.5% (magnification is ten times).

Figure 13 presents the crack distribution and tensile and compressive stresses at the center of the cross-sectional area. In terms of the crack distribution inside the aggregate, cracks are initiated in the aggregate along the surface for the boundary and layer models (ortho-radial cracks in the aggregate), while the circumferential cracks in the aggregate cannot be observed for the inner model before high expansion levels. Because the cumulative applied strain increases, cracks passing through the aggregate are generated for the boundary model and finer cracks are generated in expansive sites for the layer model with finer cracks distributed throughout the aggregate area. In addition, cracks that propagate from the mortar to the aggregate can be observed for all cases. The mechanism for the progress of these cracks is the same as the gel pocket model described in Section 4.1.1. In terms of stress distribution, the characteristic distribution caused by different expansive sites can be observed before cracking. For the boundary and inner models, tensile stress is generated at the expansive sites and propagates to the mortar, whereas compressive stress accumulates at the inner area of the reaction rim. For the layer model, considerable levels of tensile stress are generated in the inner area of the expansive layer. Further, tensile stress propagates outside the expansive layer, whereas compressive stress is generated at the expansive layer. Therefore, the stress

state inside the aggregate before cracking can be changed because of different expansive sites. This unique stress distribution will be vital in comprehending the origin of the expansion pressure. With the accompanying crack development, the tensile and compressive stresses are gradually released. The expansion crack propagation in only one direction is because of the stress release corresponding to cracking.

Based on the analytical results of the reaction rim model, it can be confirmed that onion skin cracking [11] appears with the boundary and layer models. For the boundary model, the cracks passing through the aggregate appear when the volumetric strain reaches 0.5%.

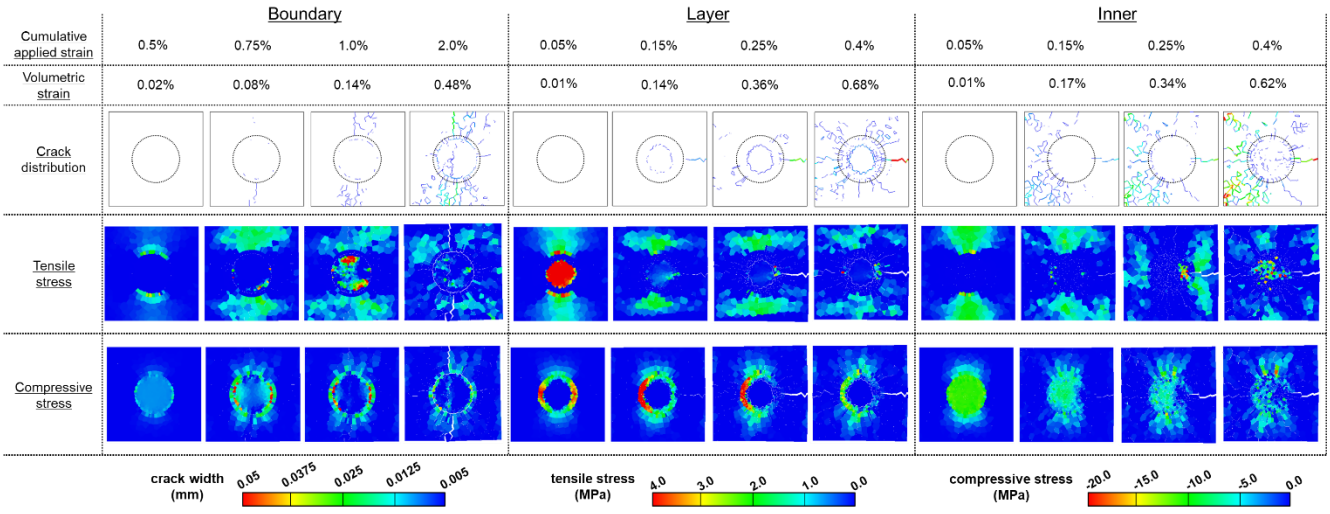

Figure 13 Crack distribution and tensile and compressive stresses at the center of the cross-sectional area of the reaction rim model for the single aggregate model (magnification of deformation is ten times). The black broken line indicates the boundary surface of the aggregate. The four cumulative applied strain stages represent results before cracking, at the generation of cracking, after crack propagation, and after volumetric strain reaches approximately 0.5%.

4.2 Analytical results of the multi-aggregate model

4.2.1 Comparison between the single aggregate and multi-aggregate models

The differences in volumetric evolution and crack distribution obtained with the single

aggregate and multi-aggregate models are compared based on the expansion level, deformation, and crack distributions at the center of their cross-sectional areas.

For the volumetric strain (Figure 14 (a)), expansions obtained with the gel pocket model for the multi-aggregate model are greater than those obtained with the single aggregate model. The difference between single and multi-aggregate models decreases with the increasing expansive site ratio. For a reaction rim model (Figure 14 (b)), the volumetric strain of the boundary model for the multi-aggregate model is greater than the expansion of the single aggregate model, whereas the volumetric strains of the other models are not affected by the number of reactive aggregates.

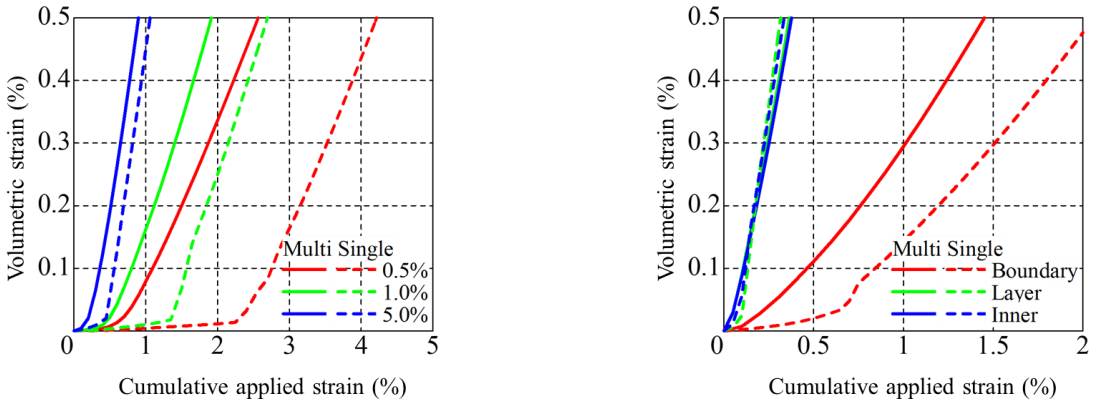

(a) Gel pocket model (b) Reaction rim model

Figure 14 Comparison of volumetric strain evolution between the single aggregate and multi-aggregate models for both expansion models.

According to the surface crack distribution (Figures 9, 12, and 15), the superficial cracks of the multi-aggregate model are distributed in all directions, whereas the single aggregate model predicts cracks orientated in a single direction; this is because multiple aggregates are randomly arranged in space. The number of surface cracks in the gel pocket model increases with increasing expansive site ratio, while that of the reaction rim model is unaffected by the

580 difference in the expansive site ratio. The explanation for the difference between the single and
581 multi-aggregate models is more pronounced for the gel pocket model as follows. The number
582 of cracks is reduced when the expansive site ratio is smaller as the expansive sites are more
583 localized. In the multi-aggregate model, cracks connected to adjacent aggregates can be
584 observed. These cracks are generated because of the interaction of stresses between adjacent
585 aggregates. Considering these features, the contribution of the cracks connecting adjacent
586 aggregates becomes more pronounced when the expansive site ratio is less.

587

588

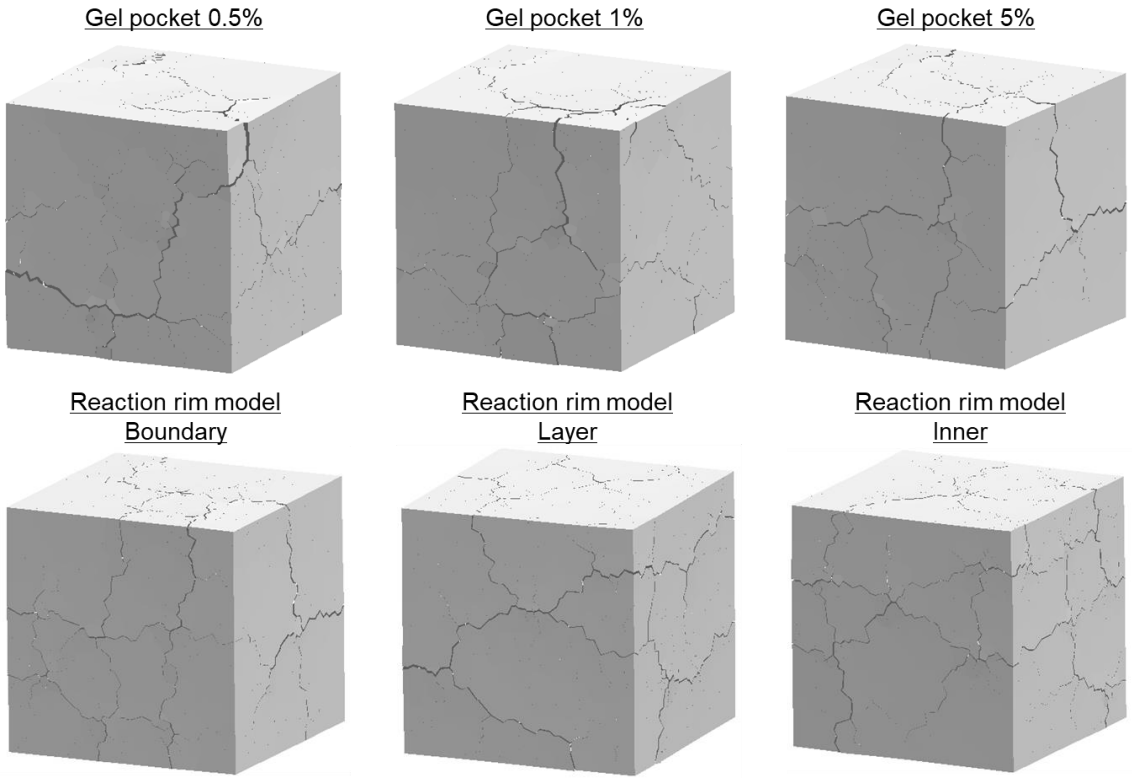

589

590 Figure 15 Deformation of the multi-aggregate model when the volumetric strain reaches approximately
591 0.5% (magnification is five times).

592

593 In addition, with respect to the crack distribution at the center of the cross-sectional area
594 (Figures 10, 13, and 16), the expansion cracks inside the aggregate for the multi-aggregate

model developed in the same manner as the single aggregate model. However, cracks propagated between adjacent aggregates for the multi-aggregate model, whereas cracks propagating from the mortar to the aggregate are observed for the single aggregate model. According to the tensile and compressive stress distributions at the center of the cross-sectional area (Figures 10, 13, and 16), the stress distribution is influenced by multiple aggregates. Before cracking, the compressive stress distributions for all expansion models are similar to those of the single aggregate model. The tensile stress is dispersed and propagates in the mortar phase for the gel pocket model, whereas it propagates between adjacent aggregates to become connected in the reaction rim model. This is caused by the random arrangement of multiple aggregates. In particular, stresses decrease gradually, thereby corresponding to the development of cracks between aggregates.

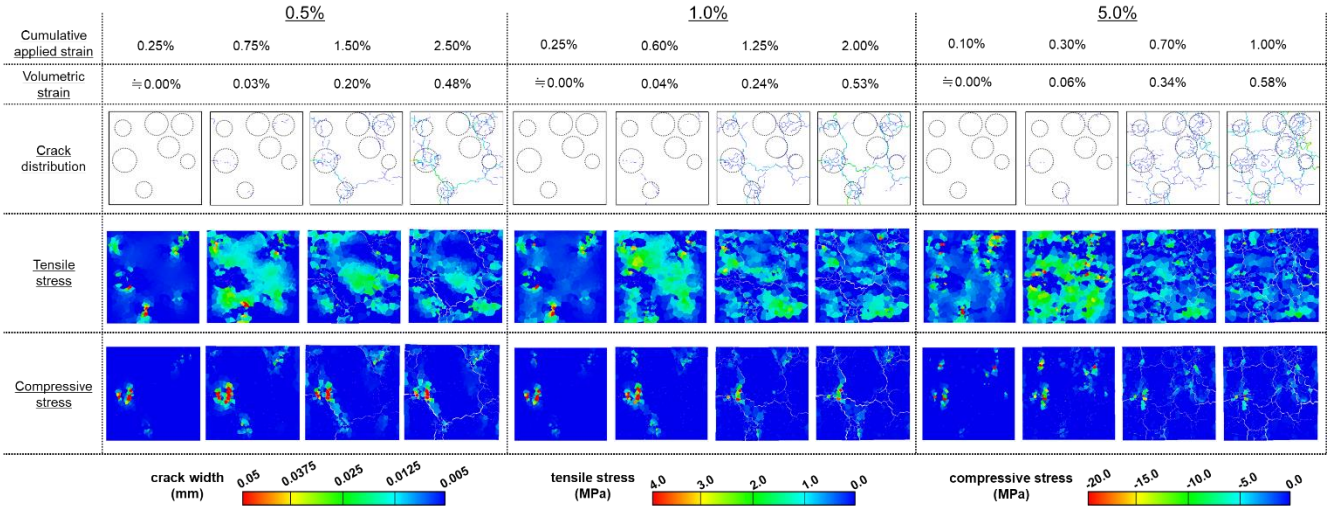

(a) Gel pocket model

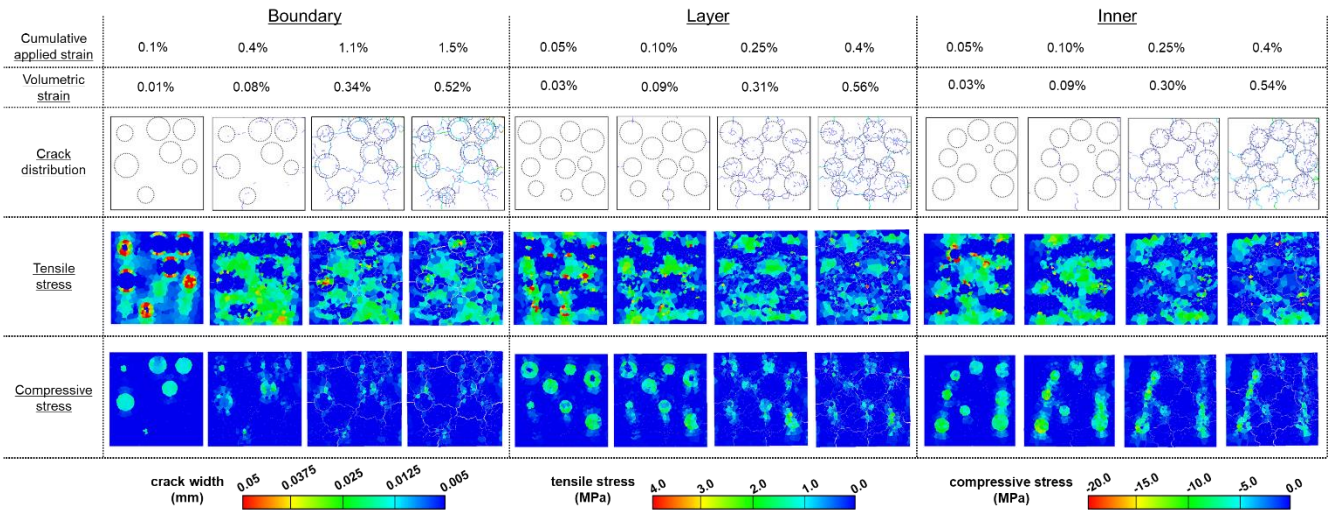

(b) Reaction rim model

Figure 16 Crack distribution, and tensile and compressive stress distributions at the center of the cross-sectional area of the multi-aggregate model (magnification of deformation is ten times). The black broken line indicates the boundary surface of the aggregate. The four cumulative applied strain stages represent results before cracking, at the generation of cracking, after crack propagation, and after volumetric strain reaches approximately 0.5%.

Based on these analytical results, the volumetric strain developed because it was influenced only by the small expansive site ratio and the boundary model, which might be attributable to the occurrence of cracks between aggregates. The small expansive site ratio in the gel pocket and boundary models are likely to generate fewer cracks. Therefore, the effect of the occurrence of cracks between aggregates on volumetric strain development increases. From the comparison between the single and multi-aggregate models, it can be observed that for the multi-aggregate model, the cracks between adjacent aggregates can be generated and accompanied by cracks inside the aggregates. These cracks would accelerate volumetric strain development even if the expansive sites are identical. Thus, for the single aggregate model, cracks propagating from the mortar to the aggregate can appear as the stress transfers from the expansive site is not inhibited. For the multi-aggregate model, the stress is nonuniformly distributed because of adjacent aggregates and the cracks connecting them. Furthermore,

crack propagation from the expansive site in the aggregates into the mortar tends to be arrested by adjacent aggregates. Because of this interference of adjacent aggregates, the crack orientation changes and the macroscopic expansion becomes isotropic.

4.2.2 Effect of the distribution of the expansive sites within the aggregate on expansion

The effect of the distribution of the expansive sites within the aggregate on the expansion behaviors is discussed based on the analytical results of the expansion evolution and crack volume (Figures 17–20). The expansion evolution (Figures 17 and 18) clearly indicates that the scattering of the expansion results obtained by the multi-aggregate model is less than that obtained by the single aggregate model. In the case of the gel pocket model, the range of the variation of expansion ranges from 0.15% to 0.20% at the maximum cumulative applied strain and the expansions in all directions change in the same manner; however, for the reaction rim model, the variation of expansion is very small and within 0.10%. Figures 17 and 18 highlight the difference in the expansions obtained by the different models as the ratio of expansive sites is higher in the layer and inner models, and the applied strains have to be smaller to obtain the same macroscopic expansion. This study focuses on the mechanical aspects, and all expansive sites are supposed to be exerted on by the same expansion. In reality, the volume of expansive sites leading to the expansion depends on chemical conditions (alkali, water, calcium, etc.) and a large quantity of reactive silica cannot alone lead to a large expansion. The consequences of reactant supply to reactive silica should be considered in future research to obtain a comparable volume of expansive sites. In the following discussion, a comparison with literature is presented based on the cracking observations obtained for a particular level of macroscopic expansion; however, the volume of expansive sites necessary

to obtain the level of expansion is not considered in the comparison.

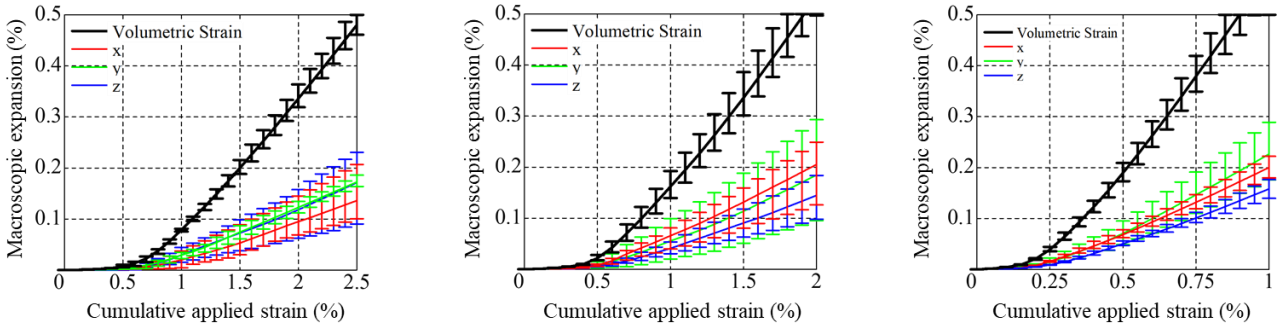

(a) 0.5% (b) 1.0% (c) 5.0%

Figure 17 Concrete expansion evolution with cumulative applied strain of expansive sites for the gel pocket model in the case of the multi-aggregate model. The error bars are calculated from three different analytical meshes.

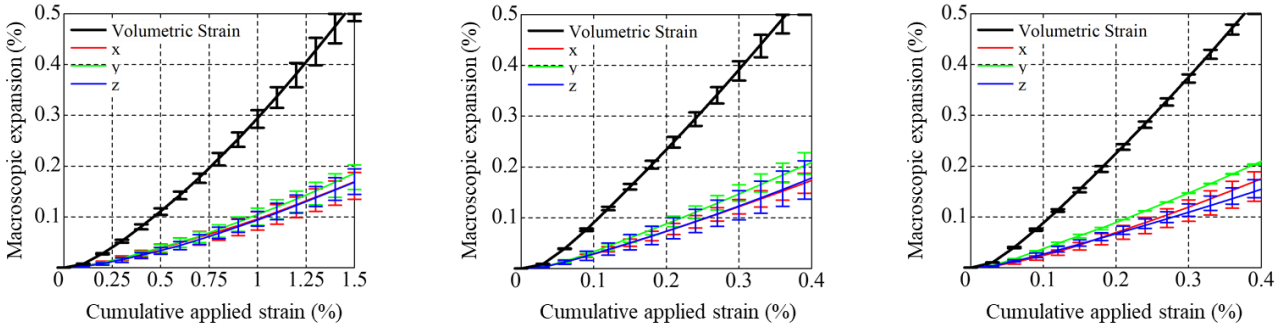

(a) Boundary model (b) Layer model (c) Inner model

Figure 18 Concrete expansion evolution with the cumulative applied strain of expansive sites for the reaction rim model in the case of the multi-aggregate model. The error bars are calculated from three different analytical meshes.

Further, it is possible to deduce the volume of the cracks with different opening widths for the two expansion models. Figures 19 and 20 show crack volume development with the cumulative applied strain for the gel pocket and reaction rim models, respectively. The opening of most cracks lies between 5 and 50 µm for the two expansion models. The gel pocket model had some cracks with openings between 50 and 100 µm and some cracks with openings

greater than 100 μm; such cracks are scarce for the numerical results obtained with the reaction rim model. The scatter of the crack volume results for all cases is remarkably lower than the variation in the macroscopic expansion, which suggests that the crack volume is independent of the arrangement of aggregates even for varying crack distribution. This leads to scattered expansion caused by the distribution of the expansive sites within the aggregate. Therefore, the expansion is almost isotropic and slightly anisotropic for the reaction rim and gel pocket models, respectively. In particular, the variation of expansion for the reaction rim model is less; the variation in the crack volume is very small because of the uniformly distributed expansive sites inside the aggregate. In the multi-aggregate model, cracks induced by the ASR can be arrested by the presence of other aggregates, and it cannot propagate freely in one direction, which is similar to a single aggregate model. Once crack propagation is prevented by adjacent aggregates, new cracks can propagate in other directions, thereby leading to cracks in all directions (Figure 15) and to expansions that are almost isotropic (Figures 17 and 18), in contrast to results obtained with a single aggregate model. This is a key conclusion and shows the importance of modeling the distribution of the aggregate in concrete to capture the ASR mechanisms at the mesoscale.

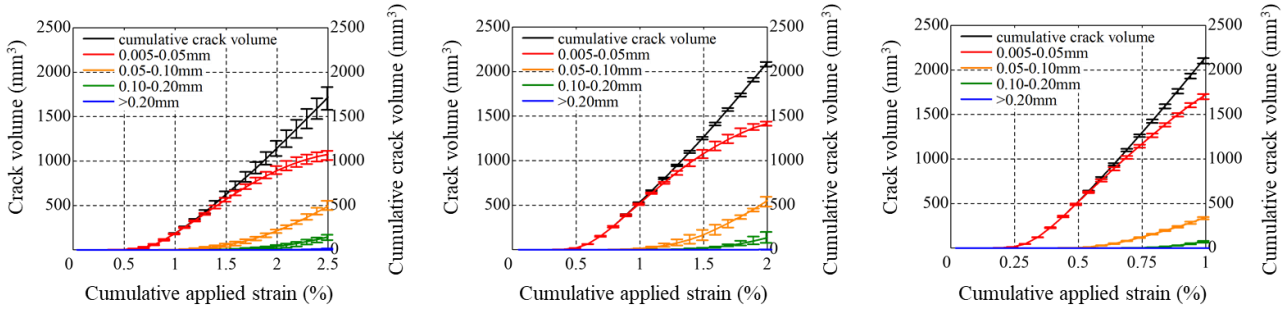

(a) 0.5% (b) 1.0% (c) 5.0%

Figure 19 Crack volume development of the gel pocket model in the case of the multi-aggregate model when the expansion strain reaches approximately 0.5%. The objective crack width is 0.005–0.05, 0.05–0.10, 0.10–0.20, and larger than 0.20 mm.

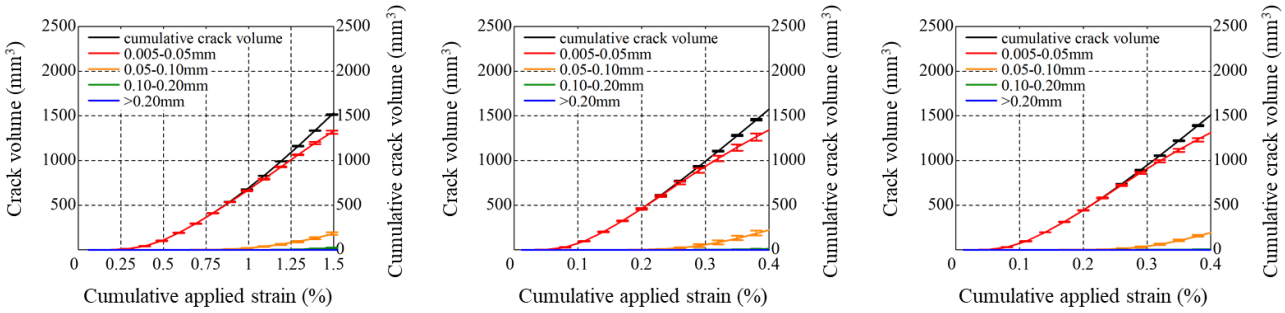

(a) Boundary model (b) Layer model (c) Inner model

Figure 20 Crack volume development of the reaction rim model in the case of the multi-aggregate model when the expansion strain reaches approximately 0.5%. The objective crack width is 0.005–0.05, 0.05–0.10, 0.10–0.20, and larger than 0.20 mm.

5. Discussion

5.1 Synthesis of numerical results

In this analysis, the change in the expansion cracking process caused by different expansive sites inside the aggregate based on the gel pocket and reaction rim models was evaluated via mesoscale discrete modeling from a mechanical standpoint and neglecting time-dependent behavior. In the gel pocket model proposed by Dunant and Scrivener [5], the expansive site was randomly arranged inside the aggregate with different expansive site ratios (Figure 4). In the reaction rim model proposed by Ichikawa et al. [4], three expansion models were constructed assuming that expansion pressure was generated inside the reaction rim produced at the inner surface of the aggregate (Figure 5). These expansion models represented two expansion cases. According to the analytical results obtained with the multi-aggregate model, the cracks inside the aggregate developed and propagated between adjacent aggregates in the gel pocket model, and the cracks inside the aggregate became pronounced when the ratio increased. For the boundary model of the reaction rim model, the cracks propagated along the interface of the aggregate, and the cracks passing through the

712 aggregate were generated as the expansion progressed. Further, in the layer and inner models
713 of the reaction rim model, many cracks appeared in the inner area of the reaction rim.
714 Furthermore, cracks were generated between adjacent aggregates in the multi-aggregate
715 model for both expansion models.
716
717 **5.2 Comparison with experimental observations**
718 The expansion cracking patterns based on the macroscopic expansion calculated by
719 this analysis are compared with experimental observations. The analytical results of the crack
720 propagation process were compared to Sanchez et al.'s model [11]. Sanchez et al. proposed
721 a qualitative AAR damage model to describe the propagation process of sharp and onion skin
722 cracks inside aggregates at several stages of macroscopic expansion (0.05, 0.12, 0.20, and
723 0.30%). There are two problems when comparing their observations and the analytical results:
724 the definitions of crack width and expansion.
725 The problem with defining the crack width is determining what part of cracks obtained
726 by modeling can be observed experimentally. In general, the minimum visible crack width
727 observable by the naked eye is considered approximately 0.05 mm. In this work, Sanchez et
728 al. used stereomicroscopy, and therefore, the minimum crack width should be smaller than
729 0.05 mm. For comparison, the authors investigated the change in the numerical crack
730 development process caused by the difference in the observable minimum crack width (Figure
731 21). The minimum crack width captured by the damage rating index (DRI) using
732 stereomicroscopy in Sanchez et al.'s work (the magnification of the microscope was 15 times)
733 was assumed to be between 0.003 and 0.005 mm (from a rough evaluation of 0.05 mm / 15
734 and personal communication with Prof. Fournier). The parametric analysis was thus performed

735 with three minimum crack widths (0.005, 0.020, and 0.050 mm). The results of this analysis are
736 shown in Figure 21, where the impact of the minimum crack width on the observations is clearly
737 highlighted. Even though it is difficult to define the minimum crack width, the crack development
738 process from the aggregate to the mortar phase is more precise for a smaller minimum crack
739 width. In this study, the minimum crack width was selected to be equal to 0.02 mm, which
740 seems to be an appropriate intermediate value. The following comparison with the
741 experimental observation performed by Sanchez et al. is based on this assumption. The
742 accuracy of the exact crack width is an important parameter to confirm the reasonability of the
743 proposed model. The validation of the minimal crack width needs to be conducted in future
744 research.
745

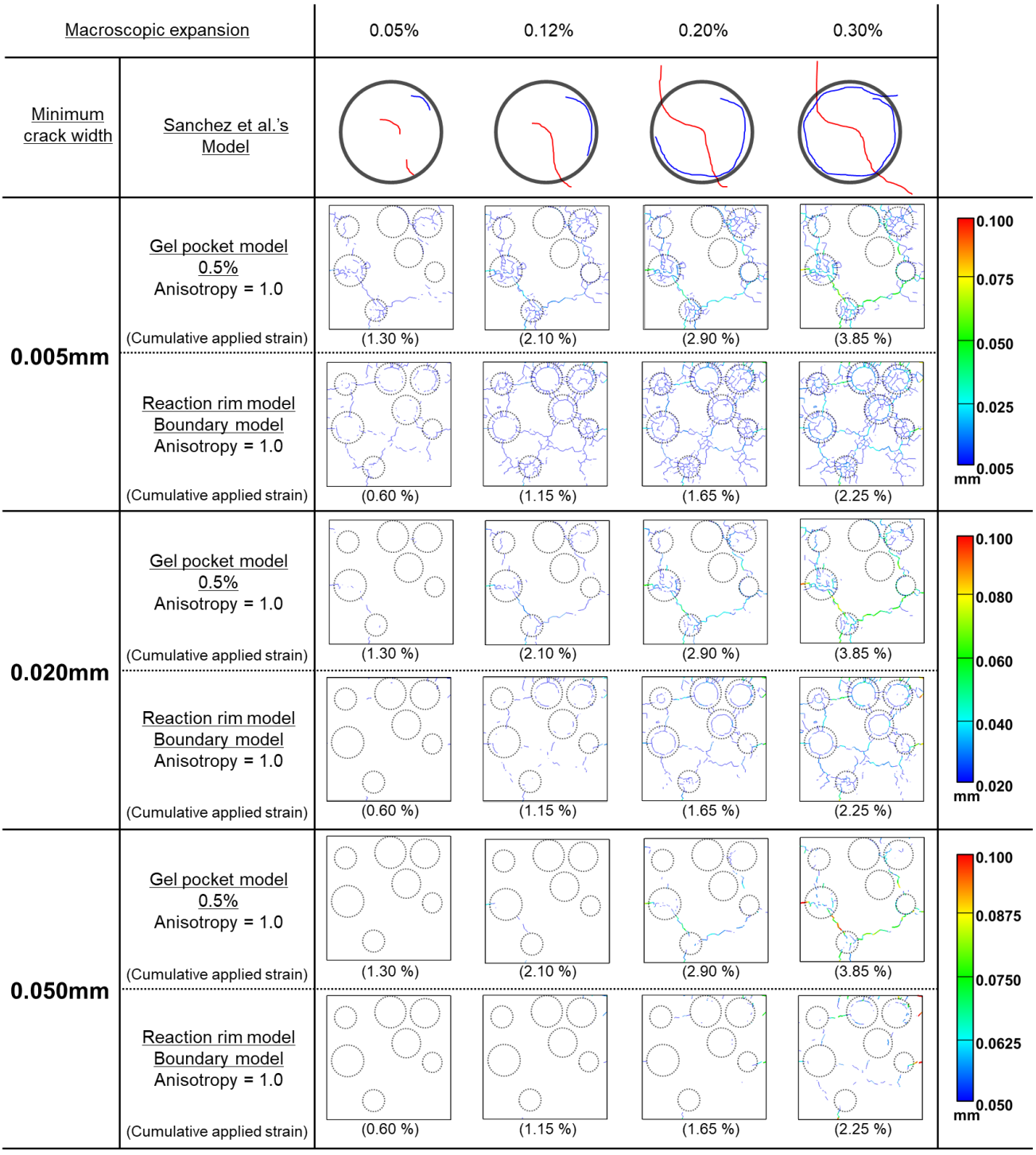

Figure 21 Verification of the effect of minimum crack width on the expansion crack propagation process of the multi-aggregate model with Sanchez et al.'s model. For this model, the red and blue lines represent "sharp cracks" and "onion skin cracks", respectively.

In terms of expansion, the expansion reported in [11] was measured in the longitudinal

752 direction of the cylindrical specimen. The ASR expansions measured in specimens can have
753 anisotropy based on the casting direction. For cylindrical and prismatic specimens, the
754 anisotropy is approximately 1.5–2.8 and 1.0–2.5 for cylindrical [38, 39] and prismatic
755 specimens [38, 40], respectively. These varied results can be attributed to the spatial
756 localization of the aggregates that are greatly influenced by the casting procedures; thus, the
757 anisotropy varies with the shape of the specimens. Owing to this anisotropy, the volumetric
758 strain of the cylindrical specimen is smaller than that of isotropic materials (three times the
759 longitudinal expansion). Thus, the following two assumptions were considered for the definition
760 of expansion:

761 - The expansion is isotropic in [11]: The volumetric expansion is equal to three times the
762 longitudinal expansion.
763 - The expansion is anisotropic in the experimental work: The volumetric expansion is
764 assumed to be equal to twice the longitudinal expansion (corresponding to an anisotropy
765 of approximately 2 between the longitudinal and transversal expansions).

766 Figure 22 presents the corresponding crack propagation process inside the aggregate
767 based on Sanchez et al.'s model and the analytical results of the gel pocket and reaction rim
768 models. The expansive site ratio is 0.5% for the gel pocket model, and the expansive site for
769 the reaction rim model is based on the boundary model. From the two assumptions above, the
770 corresponding cumulative applied strain to the macroscopic expansion of Sanchez et al.'s
771 model is different. Thus, the corresponding cumulative applied strain decreases as the
772 anisotropy increases. The target expansion is calculated by the expansion of the isotropic
773 expansion multiplied by the anisotropy, and it is consistent with the longitudinal expansion of
774 the cylindrical specimen.

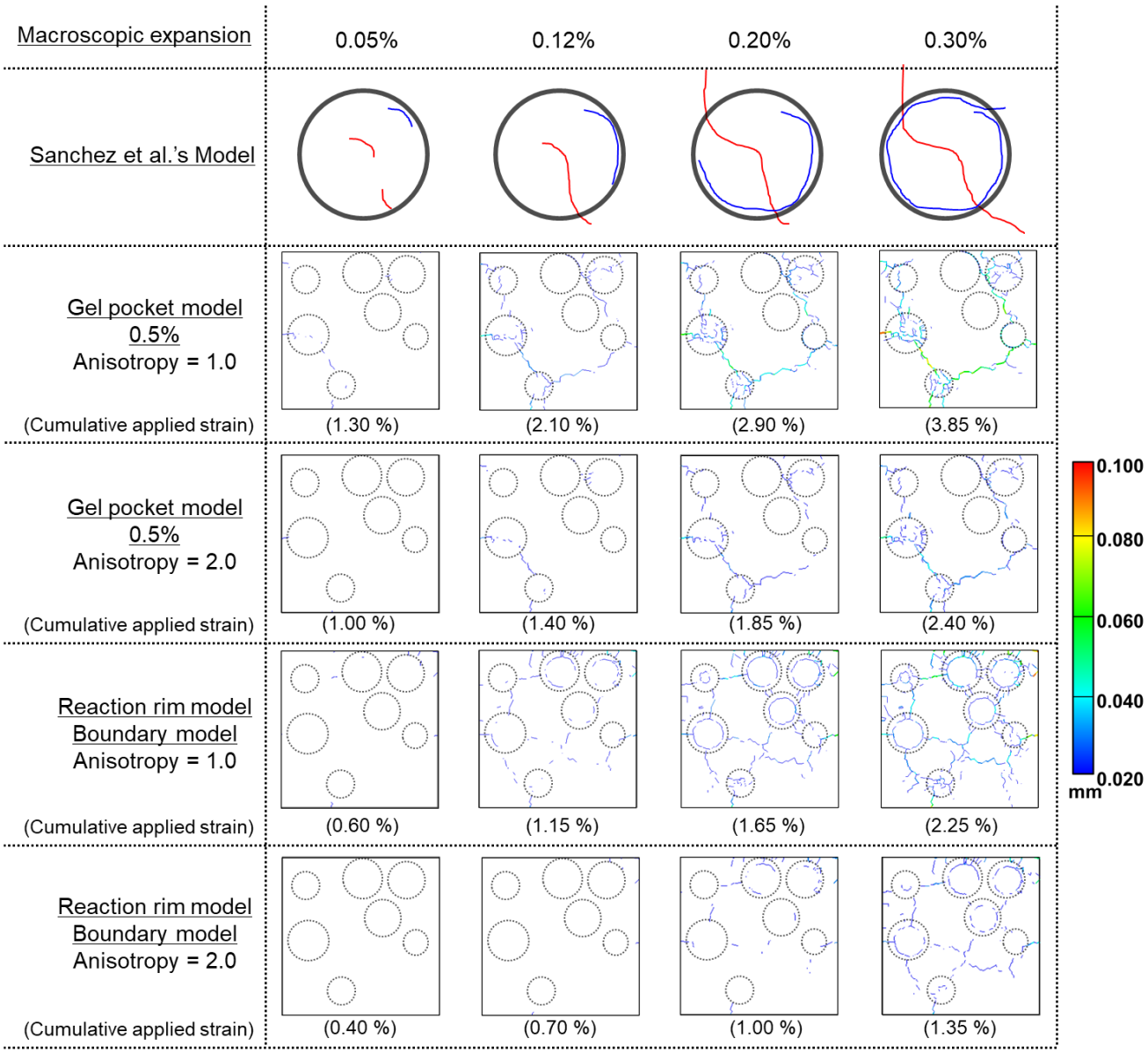

Figure 22 Validation of the expansion crack propagation process of the multi-aggregate model with Sanchez et al.'s model (minimum crack width: 0.020 mm). For an anisotropy of 1.0, the expansion strain of this model was calculated by the average expansion strain in the three directions. For an anisotropy of 2.0, the expansion strain of the Sanchez et al.'s model was calculated by twice the average expansion strain in the three directions.

In the case of the gel pocket model, the crack pattern corresponds to sharp cracking, whereas for the boundary model, the crack pattern corresponds to onion skin cracking. In the

two cases, the crack process for an anisotropy of 1.0 is overestimated, while the crack process is close to Sanchez et al.'s model for an assumed anisotropy of 2.0. Thus, the crack pattern is changed because of the different expansive sites, and the crack process is consistent with experimental observations. This suggests that sharp and onion skin cracks can be explained by gel pocket and reaction rim models on the basis of mechanics. The gel pocket model can reproduce sharp cracks, and the reaction rim model can completely reproduce onion skin cracks with some rare sharp cracks.

5.3 New insight on the mechanisms of microscopic ASR cracking

5.3.1 Microscopic observations in the literature

In actual ASR expansion, various factors related to the ASR gel production process and expansion manifestation process can impact the crack pattern. In the ASR gel production process, the production area and physical properties of ASR gel can be changed by alkali metal ion diffusion, reactions between alkali and calcium, and the distribution of the reactive silica inside the aggregates such as in veins and porous areas. With respect to the expansion manifestation process, the origin of expansion and the propagation direction of the expansion cracks can be influenced by the existence of defects inside the aggregate and their shape and distribution, reaction rim formation, bond between aggregate and cement paste/mortar, constraints applied, and aggregate shape and size distribution. Among them, the factors of influence related to the inherent characteristics of the aggregate can be the diffusion properties, distribution of the reactive silica inside aggregates, and defects inside the aggregates.

From these features of aggregates, the relationships between rock types and crack patterns from previous studies are summarized in Table 4. The overall target investigations

were 13 studies from various countries (Ben Haha et al. [6], Leemann et al. [41, 42], Chappex et al. [43], Fernandes [44], Bektas et al. [45], Ponce et al. [7], Sanchez et al. [11], Durand et al. [46], Shayan et al. [47], Katayama [48], Ichikawa et al. [4], Kawabata et al. [9]). Only data with corresponding relationships between the type of rock and crack pattern inside the aggregate that can be understood were extracted. In Table 4, the classification of rock type is indicated by small and large classifications obtained from the British Geological Survey [49–51]. The large rocks are classified into sedimentary, metamorphic, and volcanic rocks. Each rock type was further classified into three to five small classifications in this survey. Table 4 indicates that a sharp crack was confirmed for all rock types, and an onion skin crack was observed for a portion of the rocks. For example, sandstone and argillaceous rock (sedimentary rock) are composed of consolidated sand or silt/clay [49]. They potentially possess mechanically weakened areas, veins, and porous areas. In addition, schist (metamorphic rock) possesses foliated structures [50] and cracks easily along the weakened areas. These heterogeneous rocks can tend to have an easier occurrence of sharp cracks. Alternatively, relatively homogeneous rocks with less inherent defects can tend to have onion skin cracks such as andesite because the diffusion of alkali metal ions is dominant. Note that sharp cracks have been observed in rocks with fewer defects. For instance, chert is a nonclastic siliceous sedimentary rock with low porosity [49] and induces both crack patterns.

828 Table 4 Relationships between type of rock and crack pattern from previous investigations.

Small classification	Experimental observations											Remarks
	[6]	[41,42]	[43]	[44]	[45]	[7]	[11]	[46]	[48]	[4]	[9]	
Large classification: Sedimentary rock												
Limestone		S					S&O	S	S			Predominantly contains $CaCO_3$ (pp.8–10 [49])
Sandstone						S	S		S&O			Grain size: More than 32 μm (p.7 [49])
Argillaceous rock							S		S&O			Grain size: Less than 32 μm (p.7 [49])
Chert					S&O		S&O		S&O			Nonclastic siliceous sedimentary rock with less porosity (pp. 21–22 [49])
Shale									S			Contains organic carbon (p.16 [49])
Large classification: Metamorphic rock												
Quartzite		S		S					S			SiO_2: more than 80% (p.4 [50])
Gneiss						S&O	S&O					Heterogeneous material (p.5 [50])
Schist	S		S			S			S			Strongly foliated rock (p.5 [50])
Mylonite							S&O					Foliated cohesive rock (p.8 [50])
Large classification: Volcanic rock												
Andesite									S&O	S&O	S&O	SiO_2: more than 52% (p.13 [51])
Rhyolite							S&O		S			SiO_2: 48 - 52% (p.14 [51])
Granite				S		S						Quartz + Alkali feldspar (p.35 [51])

Note that "S": sharp crack, "O": onion skin crack, "S&O": sharp and onion skin cracks as observed in SEM images.

829

830

5.3.2 Insight from numerical mesoscale modeling

The analytical results obtained in this study suggest the possibility that sharp cracks occur after the generation of onion skin cracks in the boundary model of the reaction rim model. Therefore, sharp cracks can appear because of not only a defect or localized gel pockets, but also the location of the expansive site. The crack pattern can be changed by the aggregate shape and constraint condition because of the outer cement paste/mortar. Therefore, care must be taken to ensure that the crack pattern cannot be simply classified by the rock type; it is possible that all rocks would induce both sharp cracks and onion skin cracks. The observed crack pattern depends on which cracking mechanism occurs first. The factors of influence include the texture of the aggregate, distribution of the reactive silica, existence of defects, location of the reaction rim, aggregate shape and size distribution, and surrounding condition of the aggregate. Thus, the expansion crack induced by the ASR is changed by inherent and external factors. From previous investigations, the crack pattern can be classified into sharp or onion skin cracks [11]. In this study, it was suggested that the mechanism of the formation of the two crack patterns can be explained by the spatial location of the reactive sites in the aggregate as the origins of the expansion based on the gel pocket and reaction rim models. The gel pocket model can explain the mechanism of the sharp crack formation commonly observed for heterogeneous aggregates. The reaction rim model shows onion skin cracks, which can be observed in the homogeneous aggregate and sometimes leads to rare sharp cracks. These expansion models provide the mechanisms for varying crack patterns depending on the characteristics of the aggregate.

- For homogeneous aggregates (highly reactive aggregates such as glassy andesite), the reaction rim model provides a correct description of the aggregate attack. The ASR leads

to circumferential onion skin cracking with some sharp cracks.

- For heterogeneous aggregates (moderate and slowly reactive aggregates such as schist), the gel pocket model provides the most accurate representation of the reality of the location of reactive sites. Stress is then developed in the aggregate by varying the mechanical properties throughout the aggregate; the stress distribution is highly heterogeneous. This leads to a predominance of sharp cracks.

The different expansion models depend on the homogeneity of the aggregate, which acts on the homogeneity of the penetration of alkalis and the reactive silica distribution. Thus, the dominant expansion model can be changed based on aggregate homogeneity. If aggregate homogeneity is mild, expansion and cracking are based on the combination of both expansion models; further, a combination of cracking patterns may be present.

6. Conclusions

This study aimed to investigate the influence of the origins of expansion on the ASR crack propagation process through numerical analysis. The authors developed a mesoscale discrete model and applied it to represent concrete with aggregate particles and a mortar phase based on 3D-RBSM. With this mesoscale discrete model, the expansive sites were arranged inside the aggregate based on two ASR-expansion mechanisms from the literature (gel pocket model and reaction rim model). The ASR expansions and cracking patterns were investigated by applying strain to the expansive sites. The expansion crack propagation processes calculated by the gel pocket and reaction rim models were compared with previous experiments drawn from the literature. The findings are listed as follows:

1) Regardless of the expansion model applied in the mesoscale approach, the multi-aggregate model was found to be necessary to obtain realistic three-dimensional expansion and cracking. The single aggregate model leads to highly unstable and unique cracks propagating from the mortar to the aggregate. A realistic aggregate distribution needs to be modeled to reproduce a realistic distribution of expansion cracks for analyzing the ASR mechanisms.
2) The crack propagation process obtained with the gel pocket model has two stages: first, the cracks are generated around the expansive sites inside the aggregate, and then, they subsequently pass through the aggregate and propagate between adjacent aggregates with increasing expansion.
3) The crack propagation of the reaction rim model has two stages: first, the cracks are generated inside along the boundary of the aggregate for the boundary and layer models. Subsequently, the cracks propagate from the aggregate to the mortar with increasing expansion, and many cracks are observed at the entire aggregate area for the inner model. As the expansive sites exist locally at the external boundary of the aggregate, cracks along the boundary of the aggregate can be easily observed.
4) The crack propagation process inside the aggregate (sharp crack/onion skin crack) simulated with the gel pocket model and boundary model of the reaction rim model is consistent with the previous experimental classification proposed by Sanchez et al. [11].
5) From the summary of the relationships between rock type and crack pattern obtained from the literature, it was found that the expansion crack induced by ASR is inherently changed. For an equal level of macroscopic expansion, cracking in the aggregate and in concrete is not equal based on the distribution of reactive sites in the aggregate. This can

lead to different macroscopic damages for an equal level of expansion.

6) The two expansion models highlight the different crack patterns obtained according to the nature of the aggregate. For homogeneous aggregates (highly reactive aggregates such as glassy andesite), the reaction rim model provides a correct description of the aggregate attack. In such conditions, ASR leads to circumferential onion skin cracking and some sharp cracks. For heterogeneous aggregates (moderate and slowly reactive aggregates such as schist), the gel pocket model provides the most accurate representation of the actual location of reactive sites. Stress is then developed in the aggregate with mechanical properties varying throughout the aggregate, and the stress distribution is highly heterogeneous. This leads to a predominance of sharp cracks.

Acknowledgements

The authors would like to thank Prof. B. Fournier (Laval University) for insightful discussions about the width of cracks observed with stereomicroscope.

References

[1] Taylor H. F. W., 1997, Cement chemistry 2nd edition, Thomas Telford.

[2] Rajabipour F., Giannini E., Dunant C., Ideker J. H., Thomas M. D. A, 2015, Alkali-silica reaction: Current understanding of the reaction mechanisms and the knowledge gaps, Cement and Concrete Research, Vol. 76, pp. 130-146.

[3] Shi Z., Geng G., Leemann A., Lothenbach B., 2019, Synthesis, characterization, and water uptake property of alkali-silica reaction products, Cement and Concrete Research, Vol. 121, pp. 58-71.

[4] Ichikawa T., Miura M., 2007, Modified model of alkali-silica reaction, Cement and Concrete Research, Vol. 37, pp. 1291-1297.

[5] Dunant C., Scrivener K. L., 2010, Micro-mechanical modeling of alkali-silica-reaction-induced degradation using the AMIE framework, Cement and Concrete Research, Vol. 40, pp. 517-525.

[6] Ben Haha M., Gallucci E., Guidoum A., Scrivener K., 2007, Relation of expansion due to alkali silica reaction to the degree of reaction measured by SEM image analysis, Cement and Concrete Research, Vol. 37, pp. 1206-1214.

[7] Ponce J. M., Batic O. R., 2006, Different manifestations of the alkali-silica reaction in concrete according to the reaction kinetics of the reactive aggregate, Cement and Concrete Research, Vol. 36, pp. 1148-1156.

[8] Yamamoto Y., Nakamura H., Kuroda I., Furuya N., 2014, Crack propagation analysis of reinforced concrete wall under cyclic loading using RBSM, European Journal of Environmental and Civil Engineering, Vol. 18, No. 7, pp. 780-792.

[9] Kawabata Y., Dunant C., Yamada K., Scrivener K., 2019, Impact of temperature on expansive behavior of concrete with a highly reactive andesite due to the alkali-silica reaction, Cement and Concrete Research, Vol. 125, 105888.

[10] Shi Z., Park S., Lothenbach B., Leemann A., 2020: Formation of shlykovite and ASR-P1 in concrete under accelerated alkali-silica reaction at 60 and 80 °C, Cement and Concrete Research, Vol. 137, 106213.

943 [11] Sanchez L. F. M., Fournier B., Jolin M., Duchesne J., 2015, Reliable quantification of AAR
944 damage through assessment of the Damage Rating Index (DRI), Cement and Concrete
945 Research, Vol. 67, pp. 74-92.

946 [12] Reinhardt H. W., Mielich O., 2011, A fracture mechanics approach to the crack formation
947 in alkali-sensitive grains, Cement and Concrete Research, Vol. 41, pp. 255-262.

948 [13] Furusawa Y., Ohga H., Uomoto T., 1994, An analytical study concerning prediction of
949 concrete expansion due to alkali–silica reaction, in: Malhotra (Ed.), 3rd International
950 Conference on Durability of Concrete, Nice, France, SP 145–40, pp. 757–780.

951 [14] Poyet S., Sellier A., Capra B., Foray G., Torrenti J.-M., Cognon H., Bourdarot E., 2007,
952 Chemical modeling of alkali silica reaction: influence of the reactive aggregate size
953 distribution, Material and Structures, Vol.40, pp.229–239.

954 [15] Comi C., Fedele R., Perego U., 2009, A chemo-thermo-damage model for the analysis of
955 concrete dams affected by alkali-silica reaction, Mechanics of Materials, Vol. 41, pp. 210-
956 230.

957 [16] Charpin L., Ehrlacher A., 2014, Microporomechanics study of anisotropy of ASR under
958 loading, Cement and Concrete Research, Vol. 63, pp. 143-157.

959 [17] Takahashi Y., Ogawa S., Tanaka Y., Maekawa K., 2016, Scale-dependent ASR expansion
960 of concrete and its prediction coupled with silica gel generation and migration, Journal of
961 Advanced Concrete Technology, Vol. 14, pp. 444-463.

962 [18] Saouma V. E., Martin R. A., Hariri-Ardebili M. A., Katayama T., 2015, A mathematical
963 model for the kinetics of the alkali-silica chemical reaction, Cement and Concrete Research,
964 Vol. 68, pp. 184-195.

965 [19] Multon S., Sellier A., Cyr M., 2009, Chemo-mechanical modeling for prediction of alkali
966 silica reaction (ASR) expansion, Cement and Concrete Research, Vol. 39, pp. 490-500.

967 [20] Grimal E., Sellier A., Le Pape Y., Bourdarot E., 2008, Creep, shrinkage, and anisotropic
968 damage in alkali-aggregate reaction swelling mechanism-Part I. A constitutive model, ACI
969 Mater. J. Vol. 105, pp.227–235.

970 [21] Multon S., Sellier A., 2016, Multi-scale analysis of alkali-silica reaction (ASR): Impact of
971 alkali leaching on scale effects affecting expansion tests, Cement and Concrete Research,
972 Vol. 81, pp. 122-133.

973 [22] Dunant C. F., Scrivener K. L., 2012, Effects of aggregate size on alkali-silica-reaction
974 induced expansion, Cement and Concrete Research, Vol. 42, pp. 745-751.

975 [23] Dunant C. F., Scrivener K. L., 2012, Effects of uniaxial stress on alkali-silica reaction
976 induced expansion of concrete, Cement and Concrete Research, Vol. 42, pp. 567–576.

977 [24] Giorla A. B., Scrivener K., Dunant C., 2015, Influence of visco-elasticity on the stress
978 development induced by alkali-silica reaction, Cement and Concrete Research, Vol. 70, pp.
979 1-8.

980 [25] Alnaggar M., Cusatis G., Luzio G. D., 2013, Lattice Discrete Particle Modeling (LDPM) of
981 Alkali Silica Reaction (ASR) deterioration of concrete structures, Cement and Concrete
982 Composites, Vol. 41, pp. 45-59.

[26] Wang Y., Meng Y., Jiradilok P., Matsumoto K., Nagai K., Asamamoto S., 2019, Expansive cracking and compressive failure simulations of ASR and DEF damaged concrete using a mesoscale discrete model, Cement and Concrete Composites, Vol. 104, (https://doi.org/10.1016/j.cemconcomp.2019.103404).

[27] Iskhakov T., Timothy J. J., Meschke G., 2019, Expansion and deterioration of concrete due to ASR: Micromechanical modeling and analysis, Cement and Concrete Research, Vol. 115, pp. 507-518.

[28] Kawai T., 1978, New discrete models and their application to seismic response analysis of structure, Nuclear Engineering and Design, Vol. 48, pp. 207-229.

[29] Nakamura H., Iwamoto T., Fu L., Yamamoto Y., Miura T., Hanifi Y. G., 2018, Shear resistance mechanism evaluation of RC beams based on arch and beam actions, Journal of Advanced Concrete Technology, Vol. 16, pp. 563-576.

[30] Zhara A., Qiao D., Nakamura H., Miura T., Yamamoto Y., 2018, Development of simulation method of concrete cracking behavior and corrosion products movement due to rebar corrosion, Construction and Building Materials, Vol. 190, pp. 560-572.

[31] Yang Y., Nakamura H., Yamamoto Y., Miura T., 2020, Numerical simulation of bond degradation subjected to corrosion-induced crack by simplified rebar and interface model using RBSM, Construction and Building Materials, Vol. 247, (https://doi.org/10.1016/j.conbuildmat.2020.118602).

[32] Nakamura H., Srisoros W., Yashiro R. Kunieda M., 2006, Time-dependent structural analysis considering mass transfer to evaluate deterioration process of RC structures, Journal of Advanced Concrete Technology, Vol. 4, pp. 147-158.

[33] Miura T., Maruyama I., Nakamura H., Yamamoto Y., 2017, Feedback space of ion transfer through cracks during deterioration mortar due to sulfate attack evaluated by RBSM-Truss Network Model, Journal of Advanced Concrete Technology, Vol. 15, pp. 610-626.

[34] Thomure J., Bolander J. Jr., Kunieda M., 2001, Reducing mesh bias on fracture within Rigid-Body-Spring Networks, Structural Eng./Earthquake Eng., JSCE, Vol. 18, No. 2, pp. 95-103.

[35] JSCE, 2017, Standard Specifications for Concrete Structures -Design-.

[36] Sellier A., 2018, Anisotropic Damage and Visco-Elasto-Plasticity Applied to Multiphasic Materials. LMDC - Laboratoire Matériaux et Durabilité des Constructions de Toulouse; Université de Toulouse III - Paul Sabatier; INSA de Toulouse.

[37] Morenon P., Multon S., Sellier A., Grimal E., Hamon F., Bourdarot E., 2017, Impact of stresses and restraints on ASR expansion, Construction and Building Materials, Vol. 140, pp. 58-74.

[38] Smaoui N., Berube M.-A., Fournier B., Bissonnette B., 2004, Influence of specimen geometry, orientation of casting plane, and mode of concrete consolidation on expansion due to ASR, Cement, Concrete, and Aggregates, Vol. 26, No. 2, pp. 1-13.

[39] Multon S., Seignol J.-F., Toutlemonde F., 2005, Structural behavior of concrete beams affected by alkali-silica reaction, ACI materials journal, Vol. 102, No. 2, pp. 67-76.

[40] Tarek U. M., Hamada H., Yamaji T., 2003, Relation between strain on surface and strain over embedded steel bars in ASR affected concrete members, Journal of Advanced Concrete Technology, Vol. 1, No. 1, pp. 76-88.

[41] Leemann A., Merz., 2013, An attempt to validate the ultra-accelerated microbar and the concrete performance test with the degree of AAR-induced damage observed in concrete structures, Cement and Concrete Research, Vol. 49, pp. 29-37.

[42] Leemann A., 2017, Raman microscopy of alkali-silica reaction (ASR) products formed in concrete, Cement and Concrete Research, Vol. 102, pp. 41-47.

[43] Chappex T., Sofia L., Dunant C., Scrivener K., 2016, A robust testing protocol for the assessment of ASR reactivity of concrete, Proceedings of 15th International Conference on Alkali-Aggregate Reaction in Concrete, 15ICAAR2016_225.

[44] Fernandes I., 2009, Composition of alkali-silica reaction products at different location within concrete structure, Materials Characterization, Vol. 60, pp. 655-668.

[45] Bektas F., Turanli L., Topal T., Goncuoglu M. C., 2004, Alkali reactivity of mortars containing chert and incorporating moderate-calcium fly ash, Cement and Concrete Research, Vol. 34, pp. 2009-2214.

[46] Durand B., Fournier B., 2016, 20-year results of an in-situ monitoring study of large concrete electrical tower foundations affected by alkali-silica reaction (ASR), Proceedings of 15th International Conference on Alkali-Aggregate Reaction in Concrete, 15ICAAR2016_195.

[47] Shayan A., Al-Mahaidi R., Xu A., 2008, Durability and strength assessment of AAR-affected bridge deck planks, Proceedings of 13th International Conference on Alkali-Aggregate Reaction in Concrete, pp. 422-433.

[48] Katayama T., 1997, Petrography of alkali-aggregate reactions in concrete—reactive minerals and reaction products, Proceedings of East Asia Alkali-Aggregate Reaction Seminar, pp. A45-A59.

[49] Hallsworth C. R., Knox R. W. O'B, 1999, BGS Rock Classification Scheme, Volume 3, Classification of sediments and sedimentary rocks, British Geological Survey Research Report (2nd Edition), RR99-03.

[50] Robertson S., 1999, BGS Rock Classification Scheme, Volume 2, Classification of metamorphic rocks, British Geological Survey Research Report (2nd Edition), RR99-02.

[51] Gillespie M. R., Styles M. T., 1999, BGS Rock Classification Scheme, Volume 1, Classification of igneous rocks, British Geological Survey Research Report (2nd Edition), RR99-06.